WAVES IN FLUID FILLED ELASTIC TUBES

by

JOHN HENRY OLSEN
S.B., Massachusetts Institute of Technology
(1961)
M.S., Massachusetts Institute of Technology
(1963)

SUBMITTED IN PARTIAL FULFILLMENT
OF THE REQUIREMENTS FOR THE
DEGREE OF DOCTOR OF
PHILOSOPHY

at the

MASSACHUSETTS INSTITUTE OF
TECHNOLOGY

February, 1966

Signature of Author _____
Department of Mechanical Engineering, January 10, 1966

Certified by _____ 28, 1966
Thesis Supervisor

Accepted by _____
Chairman, Departmental Committee
on Graduate Students

WAVES IN FLUID FILLED ELASTIC TUBES

by

JOHN HENRY OLSEN

Submitted to the Department of Mechanical Engineering on January 10, 1966 in partial fulfillment of the requirement for the degree of Doctor of Philosophy.

ABSTRACT

Large amplitude long wavelength standing waves in liquid filled elastic tubes were studied to develop a physical model for the flow, suitable for application to the more complicated case of blood flow in the human arterial system. Accurate experiments were performed on long rubber tubes; a physical model was developed and the resulting non-linear equations were solved by two different methods. The two solution methods, a numerical integration scheme and a perturbation method, gave identical representations of the non-linear effects for the range of flow parameters found in the arterial system. Comparison of the experimental results with results from these solutions shows a considerable error for large Reynolds number motions. This error is thought to be due to the failure of the model to describe the frictional phenomena associated with entry length and turbulence. Excellent agreement was obtained for smaller amplitude motions.

Thesis Supervisor: Ascher H. Shapiro
Title: Ford Professor of Mechanical Engineering

TABLE OF CONTENTS

	ABSTRACT	1
	TABLE OF CONTENTS	2
	ACKNOWLEDGMENTS	3
	BIOGRAPHICAL NOTE	4
	LIST OF SYMBOLS	5
I	INTRODUCTION	8
II	RANGE OF INVESTIGATION	9
III	BASIC CONSIDERATIONS FROM FLUID MECHANICS	12
IV	THE TUBE LAW	16
V	THE FRICTION APPROXIMATION	24
VI	SOLUTION OF THE EQUATIONS	27
VII	EXPERIMENTAL APPARATUS AND MEASUREMENTS	44
VIII	RESULTS	53
IX	SUMMARY AND CONCLUSIONS	71
	REFERENCES	74

APPENDICES

1.	An Analysis of the Error Resulting from the Momentum Flux Approximation	75
2.	Derivation of the Characteristic Equations	79

ACKNOWLEDGMENTS

First, I would like to thank Professor A. H. Shapiro who suggested research in the area of biological fluid motions and provided excellent guidance and many helpful suggestions during the work on this project. I would also like to thank Thomas Latham and Richard Perry who helped with the experimental work. Mr. Perry worked on the viscometer and did measurements on the dynamic behavior of the tube wall material.

This work was done in part at the Computation Center at MIT, Cambridge, Massachusetts. It was supported in part by Grant #HD01288 from the National Institutes of Health, U. S. Public Health Service. It was also aided by a grant from the Massachusetts Heart Association.

BIOGRAPHICAL NOTE

The author began his technical training at Cass Technical High School in Detroit with the intention of becoming a tool and die maker. The skills he learned there proved to be useful in later experimental work in the field of fluid mechanics. He was introduced to fluid mechanics during a job connected with the MIT undergraduate cooperative course at Holley Carburetor Company. There he studied orifice flows. He has since worked on a variety of fluid mechanical problems including a Bachelor's thesis and a Master's thesis at MIT in the field of liquid metal MHD.

He received the degree of Bachelor of Science from MIT in June of 1961 and that of Master of Science, also from MIT, in June of 1963. During his years of graduate study he held the position of Research Assistant in the Department of Mechanical Engineering.

LIST OF SYMBOLS

Symbol	Definition
a	SinNXCoshNY
A	internal tube area
b	Cos NXSinhNY
C	wave speed
D	internal tube diameter
d	$CosNX(1-x_o)CoshNY(1-x_o)$
E	elastic modulus
f	$SinNX(1-x_o)CoshNY(1-x_o)$
g	$CosNX(1-x_o)SinhNY(1-x_o)$
h	tube wall thickness
i	$\sqrt{-1}$
J_1, J_2	Bessel functions
ℓ	tube length
M_{10}	see chapter 5
N	$\omega\ell/C_o$
P	pressure difference across tube wall
Q	total flow rate
r	$SinNX(1-x_o)SinhNY(1-x_o)$
R	tube internal radius
Re	Reynolds number
s	measure of steady flow

Symbol	Definition
S	dimensionless group, see chapter 6
t	time
T	$8\ Ns/\alpha^2$
v	velocity averaged across tube area
x	length coordinate
X	see equation (35)
Y	see equation (35)
α	$\sqrt{\frac{\omega R^2}{\nu}}$, or characteristic coordinate
β	characteristic coordinate
ε	Q_o/A_oC_o
ε_{10}	see chapter 5
η	dimensionless group, see chapter 6
λ	wavelength
μ (subscript)	function used in series solution
μ (no subscript)	viscosity
ν	kinematic viscosity
ξ	constant in series solution
ρ	fluid density
σ (subscript)	stress
σ (no subscript)	Poisson's ratio
τ	shear force per unit length
ϕ	A_N/A

Symbol	Definition
Φ	$(4\phi_o^2-1)/4(2\phi_o^2-1)$
ω	circular frequency of motion

Subscripts

N	denotes conditions with no pressure across table wall
o	denotes conditions with tube inflated but no motion
1,2	order of terms in series solution
α	differentiation with respect to α
β	differentiation with respect to β
θ	direction in cylindrical coordinates
r	direction in cylindrical coordinates
z	direction in cylindrical coordinates

I INTRODUCTION

The purpose of this study was to provide information relating to non-linear effects in blood flow in the human arterial system.

The present paper presents the results of a study of standing waves in a liquid-filled rubber tube. The object was to develop a theory for large amplitude oscillating flows of a viscous incompressible liquid in long elastic tubes and to test this theory with a set of accurate experiments. Standing waves were chosen for the study because of the ease of accurately prescribing the boundary conditions in the experiments. However, the analytical methods used are equally applicable to traveling waves or to any arbitrary boundary conditions at the tube ends.

The study proceeds by developing a physical model for the flow based on a long wavelength assumption. The necessary equations for describing the behavior of the model are derived at each step of development. These equations are then combined and, with the appropriate boundary conditions, are solved by several methods. First, to obtain a simple notion of the form of the solution, the results for the linear frictionless case are presented. Next, a numerical method is described where the equations are integrated stepwise along the characteristic curves. Finally, a perturbation series is described where the equations are analytically integrated along the characteristic curves. The results of these solutions are then compared with one another and with a set of experimental data.

II RANGE OF THE INVESTIGATION

1. The Possible Motions of a Tube

An elastic tube filled with an incompressible liquid can exhibit several types of wave motion. A non-axisymmetric wave can be induced by shaking the tube end transverse to its axis. A torsion wave can be produced by twisting the tube end and a stretching wave by pulling it parallel to the tube axis. Finally, a bulging wave can be induced by injecting fluid into the tube end. These motions are illustrated in fig. 1.

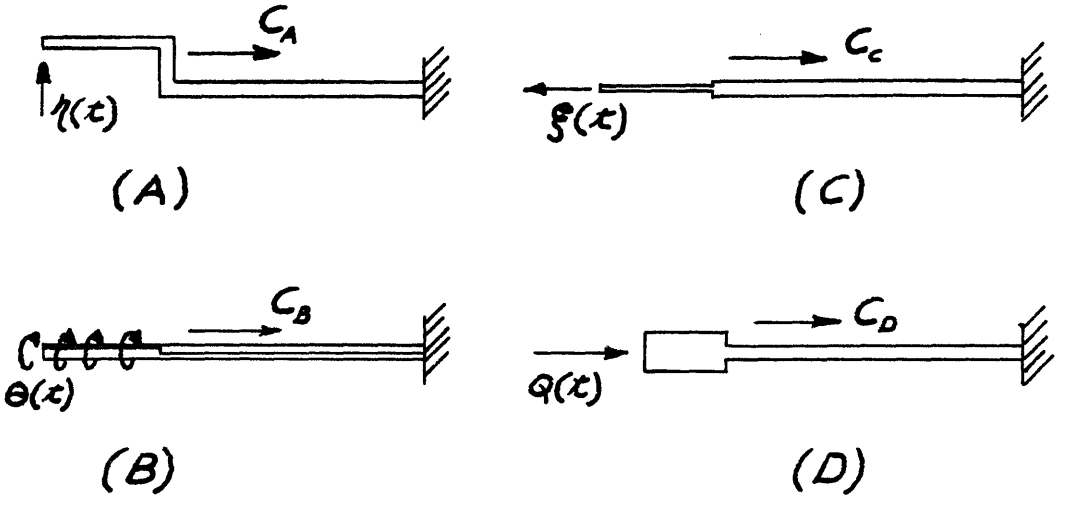

FIGURE 1

For each type of wave there is a wave speed and a corresponding set of suitable boundary conditions.

In the linear theories of both Womersley and Morgan an axisymmetric motion is treated where the tube is free to bulge and to move longitudinally.[1,2] In both works two wave speeds are found, but one wave speed and the corresponding boundary conditions are

incorrectly ignored. With only one wave speed, when the boundary conditions for pressure or flow at the ends of the tube are given, the necessary additional conditions on the longitudinal motion of ends cannot be given. If the motions in a tube, fixed at its ends, are computed while ignoring one wave speed, an excess longitudinal motion will be calculated not only in the center portions of the tube, but also at the ends where the longitudinal motion is precisely zero. For this reason the theories of Womersley and of Morgan predict an excess longitudinal motion that has not been observed.

2. The Motion to be Considered

A real artery is longitudinally constrained at points much closer than one wave length apart. As a result no longitudinal motion is observed.[3] Therefore, the tube treated in this study is not allowed to move longitudinally. A pure bulging mode, caused by the injection of fluid, is the only type of wave to be considered.

It will be shown in chapter 6 that for small amplitudes a sinusoidal excitation causes the tube to vibrate in a natural mode where motions at all points are sinusoidal functions of time. A sin ωt excitation was chosen for this study because deviations from sinusoidal motion are then due to non-linear effects only and can be used as a simple test for non-linearity.

3. Parameters for the Motion

Table I shows a comparison of the important parameters of the experimental flow with physiological values. The physiological value for ω is taken as the circular frequency of the first harmonic of the heart output.

TABLE I

Parameter	Value	Range for the Larger Human Arteries	Range for This Study
λ/R	-	greater than 100	greater than 1000
ε	Q/A_oC_o	.18-.01	.19-.007
α	$\omega R^2/\nu$	17.0-3.0	25-1.9
R_e	VD/ν	10,000-500	28,000-120
N	$\omega\ell/C_o$	not applicable	.5-14.0
s	-	.5-.1	9.0-.1
P	$P_o/\rho C_N^2$	.28	.2
h/R	-	.1	.13

No attempt was made to model the anomalous viscosity of blood. The arteries were taken to be thin-walled elastic tubes whose mechanical properties were accounted for by the quantities C_o and C_N in the above table.

III BASIC CONSIDERATIONS FROM FLUID MECHANICS

The fact that the wavelength is much greater than the tube radius (Table I) allows a very important approximation. It can be shown that for large λ/R the radial accelerations and pressure gradients are unimportant.[1] We can then formulate a one-dimensional model in which only longitudinal fluid accelerations and forces are important. To further simplify the problem we will ignore the velocity profile and consider only the mean velocity parallel to the tube axis. This approximation will be seen to introduce small errors in the non-linear terms of the momentum equation.

1. Conservation of Mass

We will begin by deriving the relation expressing conservation of mass. Consider a section of tubing between two parallel planes a distance dx apart as shown in fig. 2.

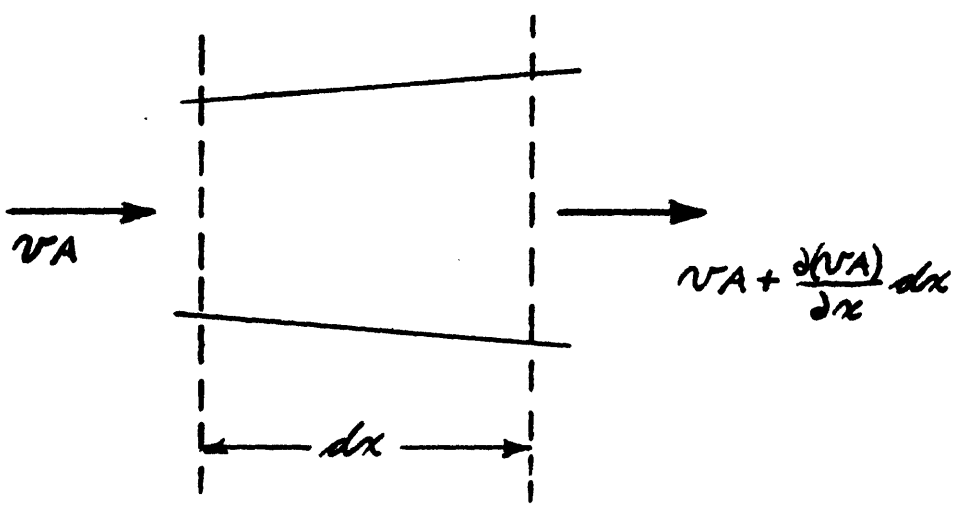

FIGURE 2

If more fluid enters at the left plane than leaves at the right plane, the volume of the tube section must increase. That is,

$$vA - \left(vA + \frac{\partial(vA)}{\partial x}dx\right) = \frac{\partial}{\partial t}(A\,dx)$$

which reduces to

$$(1) \qquad \frac{\partial(vA)}{\partial x} + \frac{\partial A}{\partial t} = 0$$

where A is the inner area of the tube normal to the axis and v is the mean fluid velocity parallel to the tube axis. This equation of conservation of mass involves no approximation.

2. Conservation of Momentum

To obtain the equation expressing conservation of momentum we will use the control volume relations. Consider a fixed control volume which at time t coincides with a short section of the tube. At time t+dt the tube has moved away from the volume. We will consider the forces and momentum fluxes acting on the control volume during this time. See fig. 3.

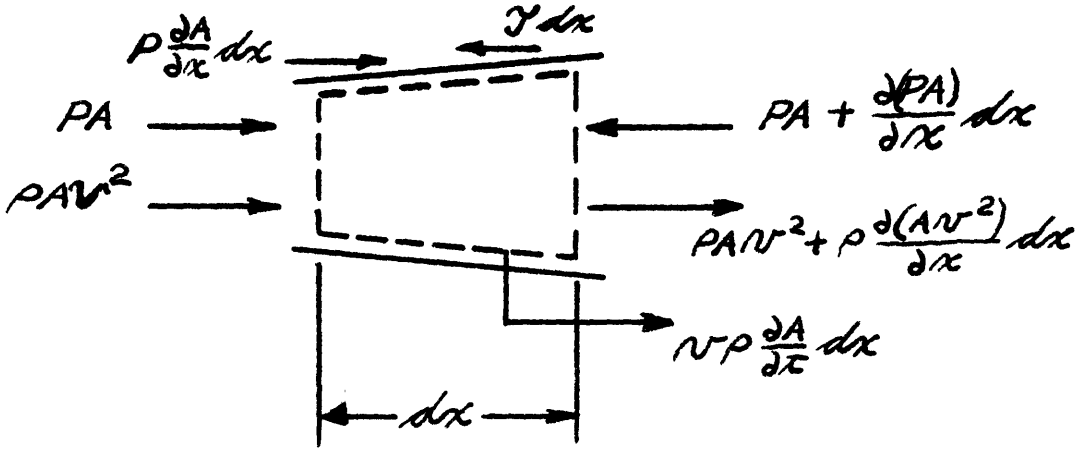

FIGURE 3

τ is the frictional shear force per unit length acting on the control volume. It will be evaluated in chapter 5. Equating forces and the momentum fluxes to the rate of change of momentum within the control volume, we arrive at the following results.

$$PA - \left(PA + \frac{\partial(PA)}{\partial x}dx\right) + P\frac{\partial A}{\partial x}dx - \tau\,dx + \rho A v^2 -$$

$$\left(\rho A v^2 + \rho\frac{\partial(Av^2)}{\partial x}dx\right) - v\rho\frac{\partial A}{\partial t}dx = \rho\frac{\partial}{\partial t}(A_c v)$$

Substituting for $\partial A/\partial t$ from eq. 1 and simplifying, we obtain

$$(2) \qquad A\frac{\partial P}{\partial x} + \rho A\frac{\partial v}{\partial t} + \rho A v\frac{\partial v}{\partial x} = -\tau$$

This relation contains an approximation. The quantities of the form ρAv^2 are equal to the true momentum flux only for a flat velocity profile. For all other profiles ρAv^2 must be regarded as an approximation. For example, the true momentum flux for the parabolic profile of poiseuille flow is $4/3\ \rho Av^2$. This is the only approximation involved and the matter is discussed in detail in appendix I.

3. <u>The Special Case when P = f(A)</u>

It will be shown in the next chapter that P can be regarded as a function of A alone when λ is large compared to R. We can then define a quantity C, which will later be identified as the wave speed, as

$$(3) \qquad C^2 \equiv \frac{A}{\rho}\frac{dP}{dA}$$

The quantity dP/dA will be determined from the pressure vs. area relation derived in the next chapter. With this definition ∂P/∂x becomes

$$\frac{\partial P}{\partial x} = \frac{dP}{dA}\frac{\partial A}{\partial x} = c^2\frac{\rho}{A}\frac{\partial A}{\partial x}$$

and after substituting into eq. (2) we obtain

$$(4) \quad c^2\frac{\partial A}{\partial x} + A\frac{\partial v}{\partial t} + Av\frac{\partial v}{\partial x} = -\frac{\gamma}{\rho}$$

IV THE TUBE LAW

The object of this section is to find the relation between P and A for a rubber tube from which to calculate the derivative dP/dA.

1. The Governing Relations

The large value of λ/R implies that the longitudinal slope and curvature of the tube wall is small. We can then regard the equilibrium of the pressurized tube as a balance between the hoop stress and internal pressure as in figure 4.

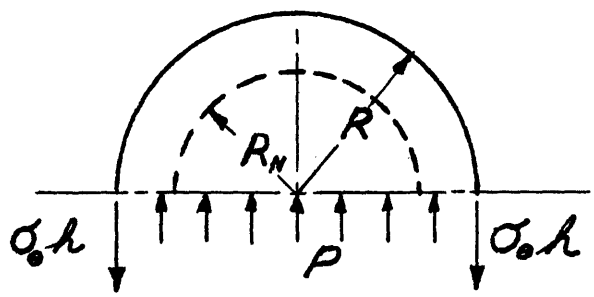

FIGURE 4

The force balance relation is

$$\sigma_\theta = PR/h$$

The condition of no longitudinal motion is that

$$\varepsilon_z = 0$$

The geometric relation for the radial strain is

$$\varepsilon_\theta = R/R_N - 1$$

Rubber behaves as a linear elastic material up to a strain of about 40%.[4] We can, therefore, use the linear elastic relations that

$$\epsilon_\theta = \frac{1}{E}(\sigma_\theta - \sigma\sigma_z)$$

$$\epsilon_z = \frac{1}{E}(\sigma_z - \sigma\sigma_\theta)$$

where σ_r has been set equal to zero because the wall is assumed thin (table I).

A further property of rubber is that the volume remains very nearly constant during deformation. Thus, h is given by

$$h = h_N \frac{R_N}{R}$$

By combining these relations and expressing the results in terms of A rather than R we obtain

$$P = 2\rho C_N^2 \left(\sqrt{\frac{A_N}{A}} - \frac{A_N}{A}\right) \tag{5}$$

$$C^2 = C_N^2 \left(2\frac{A_N}{A} - \sqrt{\frac{A_N}{A}}\right) \tag{6}$$

where

$$(7) \qquad C_N^2 \equiv \frac{E h_N}{2\rho R_N (1-\sigma^2)}$$

2. Implications for the Experiments

Notice that the quantity ρC_N^2 contains all the elastic parameters of the tube. Measurement of this quantity and ρ are the only measurements necessary to determine the wave speed in the tube. ρC_N^2 can be easily measured by taking the slope of a curve of P vs. $\left(\sqrt{\frac{A_N}{A}} - \frac{A_N}{A}\right)$. Figure 5 is such a curve made from experimental data. It shows that eq. (5) is correct within the experimental range and yields a value for PC_n^2. The experimental technique for obtaining the curve is described in chapter 7.

A plot of $P/\rho C_N^2$ vs. A/A_N, fig. 6, shows the surprising result that $P/\rho C_N^2$ has a maximum value. This maximum has important meaning for the experimenter. If the tube is held at constant volume at a large area just below the maximum point and then by chance a portion is stretched to a larger area corresponding to a lower pressure, the large portion will expand at the expense of the small portion. The expansion continues until the non-linear stress strain effects in the rubber stop it. At this point the tube has taken a permanent set and is ruined for further experiments.

The above instability places an upper limit on the working pressure in the tube. A lower limit also exists. If the pressure drops below the outside pressure, the tube collapses rather than remaining round and obeying eq. (5). The collapse introduces very large non-linear effects

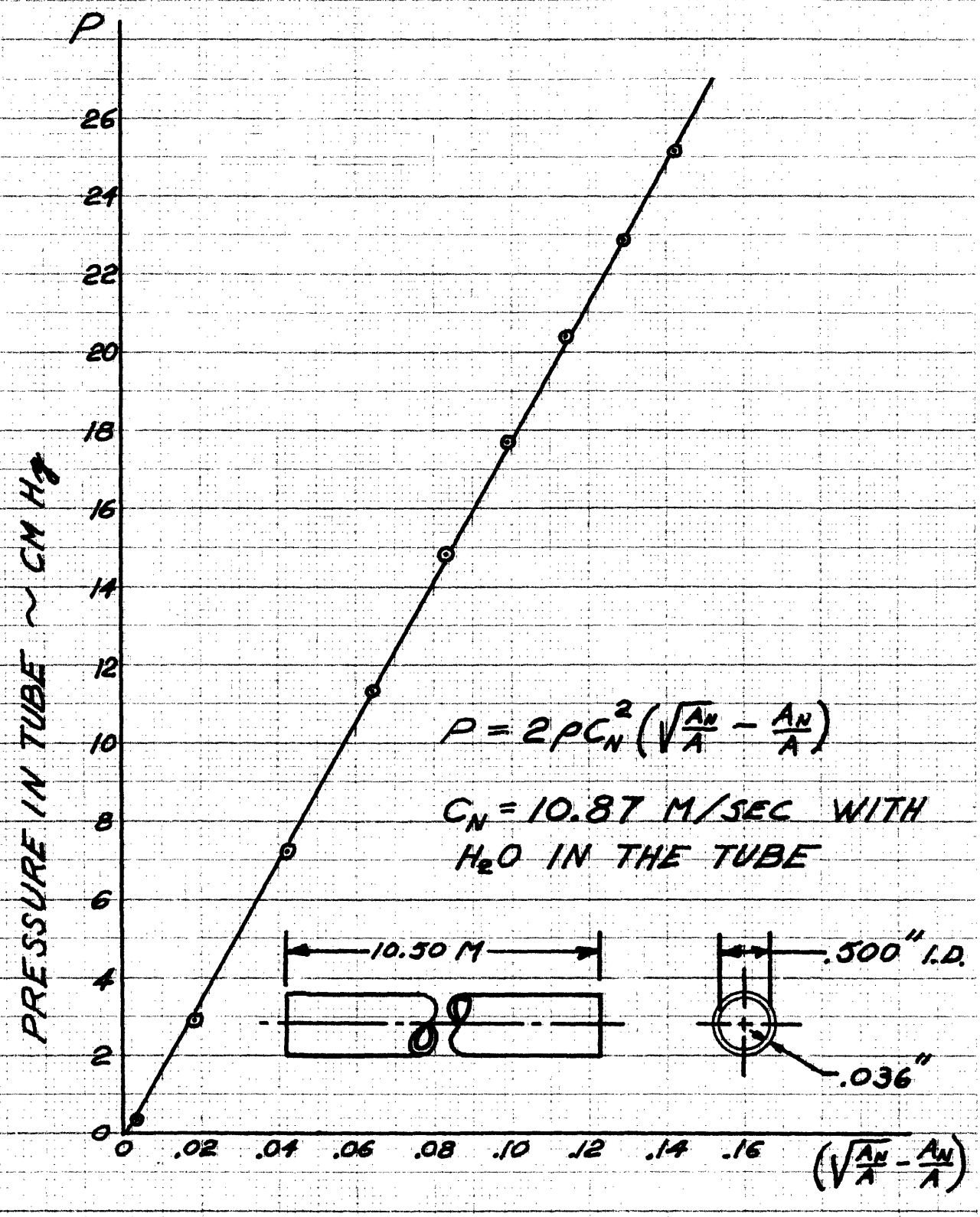

EXPERIMENTAL PRESSURE-AREA RELATION FOR A RUBBER TUBE

FIGURE 5

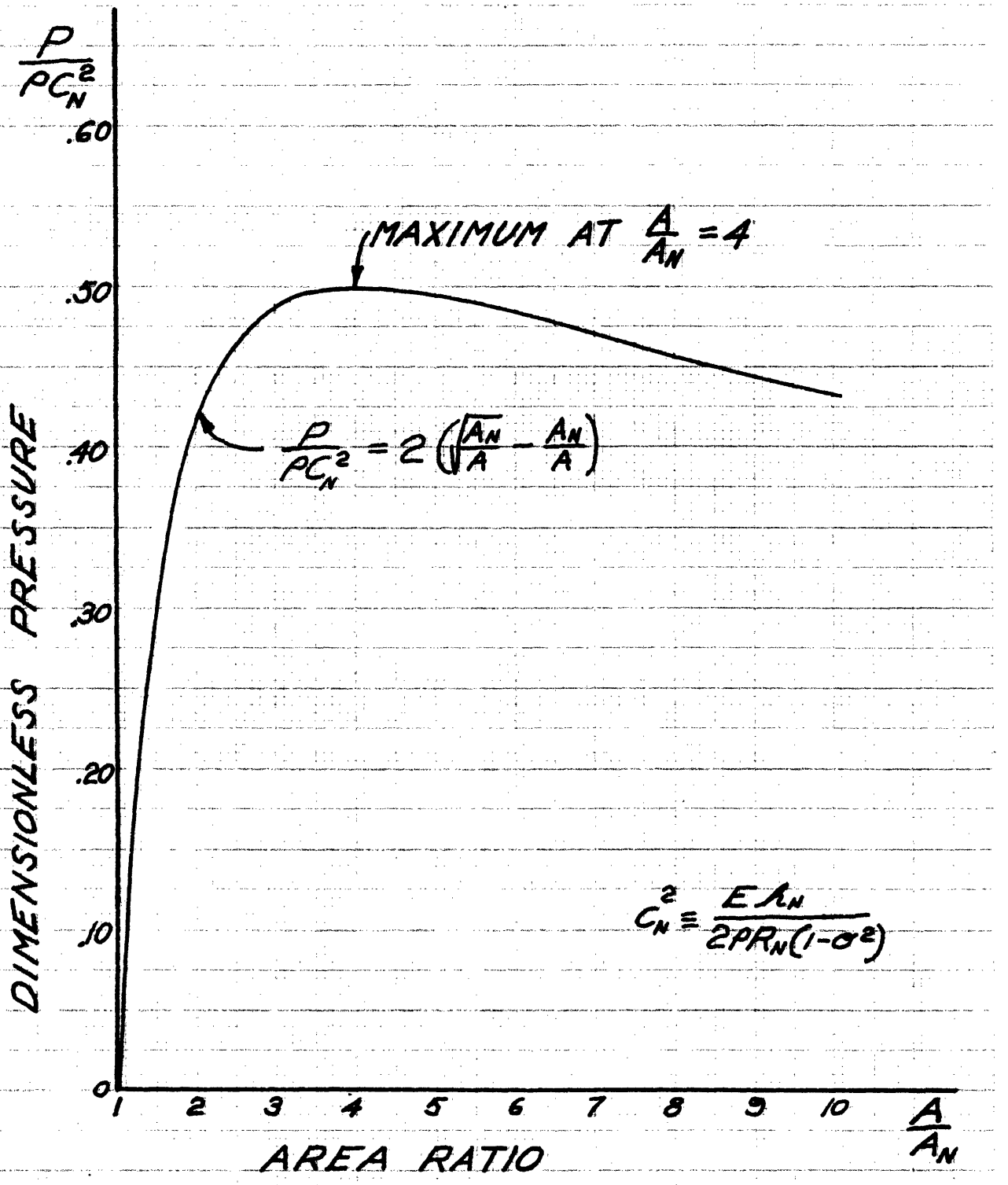

PRESSURE-AREA RELATION FOR AN ELASTIC TUBE

FIGURE 6

not observed physiologically and is to be avoided. The tube must be pressurized to a value such that the fluid motions never reduce the pressure below the external pressure.

3. The Dynamic Properties of the Tube

Figure 7 is a graph of C/C_N vs. $P/\rho C_N^2$ calculated from equations (5) and (6). We will see in chapter 6 that C is the speed of a linear frictionless wave. The experimental values of C for the plot were measured for the tube of fig. 5 by timing the motion of a very small quick pressure pulse. The experimental speed is slightly higher than the calculated speed. This small error can be related to the peculiar properties of the rubber tube material.

The elastic modulus E is slightly dependent on the frequency. Figure 8 shows the relative force resulting from stretching a strip of rubber from the experimental tube at various frequencies of sinusoidal motion but at a fixed amplitude of about 50% strain. The rubber appears stiffer at higher frequencies. In later comparisons with experimental results, C_N is adjusted upward for higher frequencies. Since E is proportional to the relative force and C_N is proportional to $\sqrt{E}$. C_N is corrected by multiplying by square root of the relative force of fig. 8.

The tube material showed negligible hysteresis effects but did exhibit a permanent strain of about 5% when stretched for the first time. After this initial set, it behaved like an ordinary elastic material except for the slight frequency dependence of E.

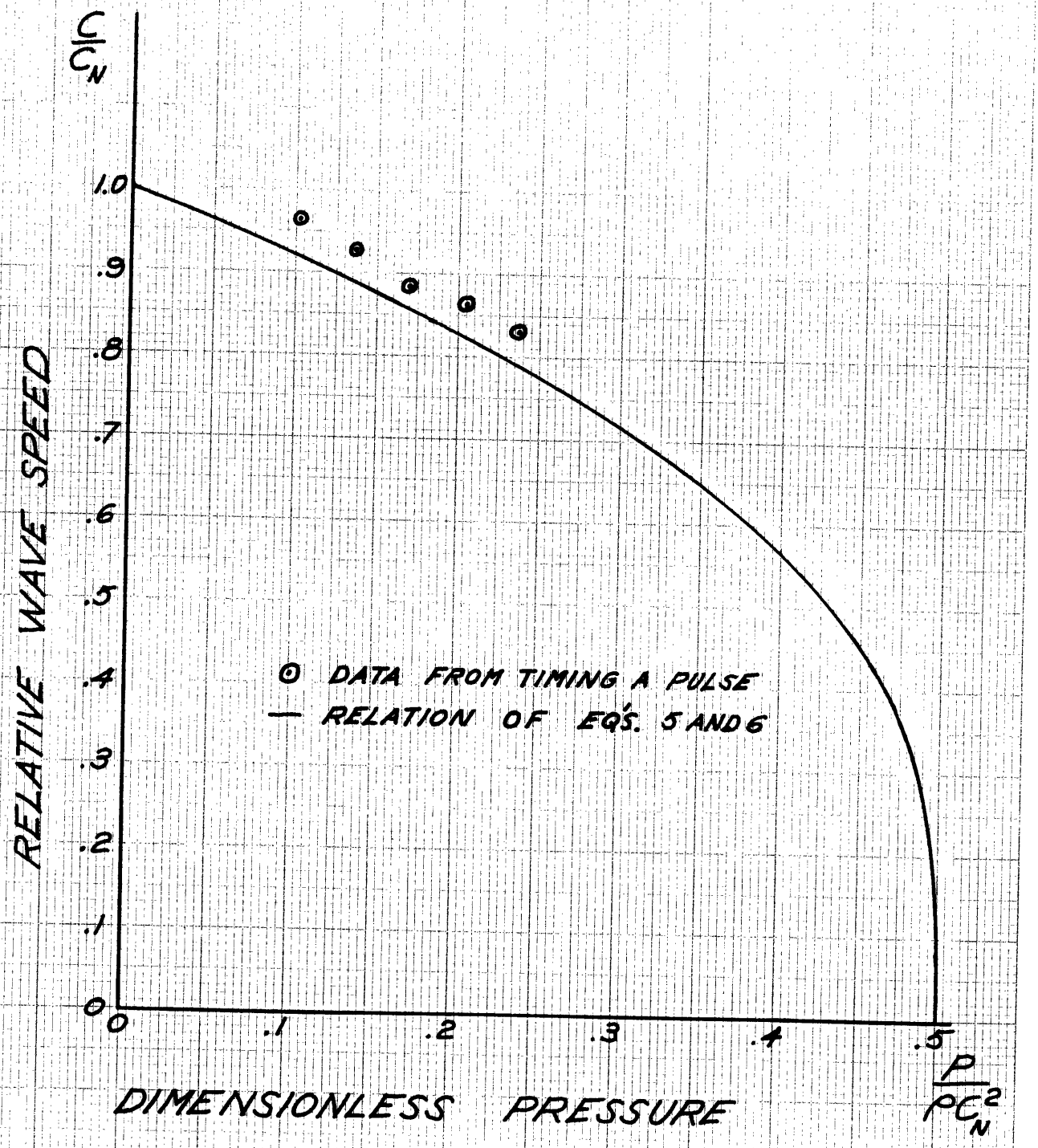

THE DEPENDENCE OF WAVE SPEED ON INTERNAL PRESSURE

FIGURE 7

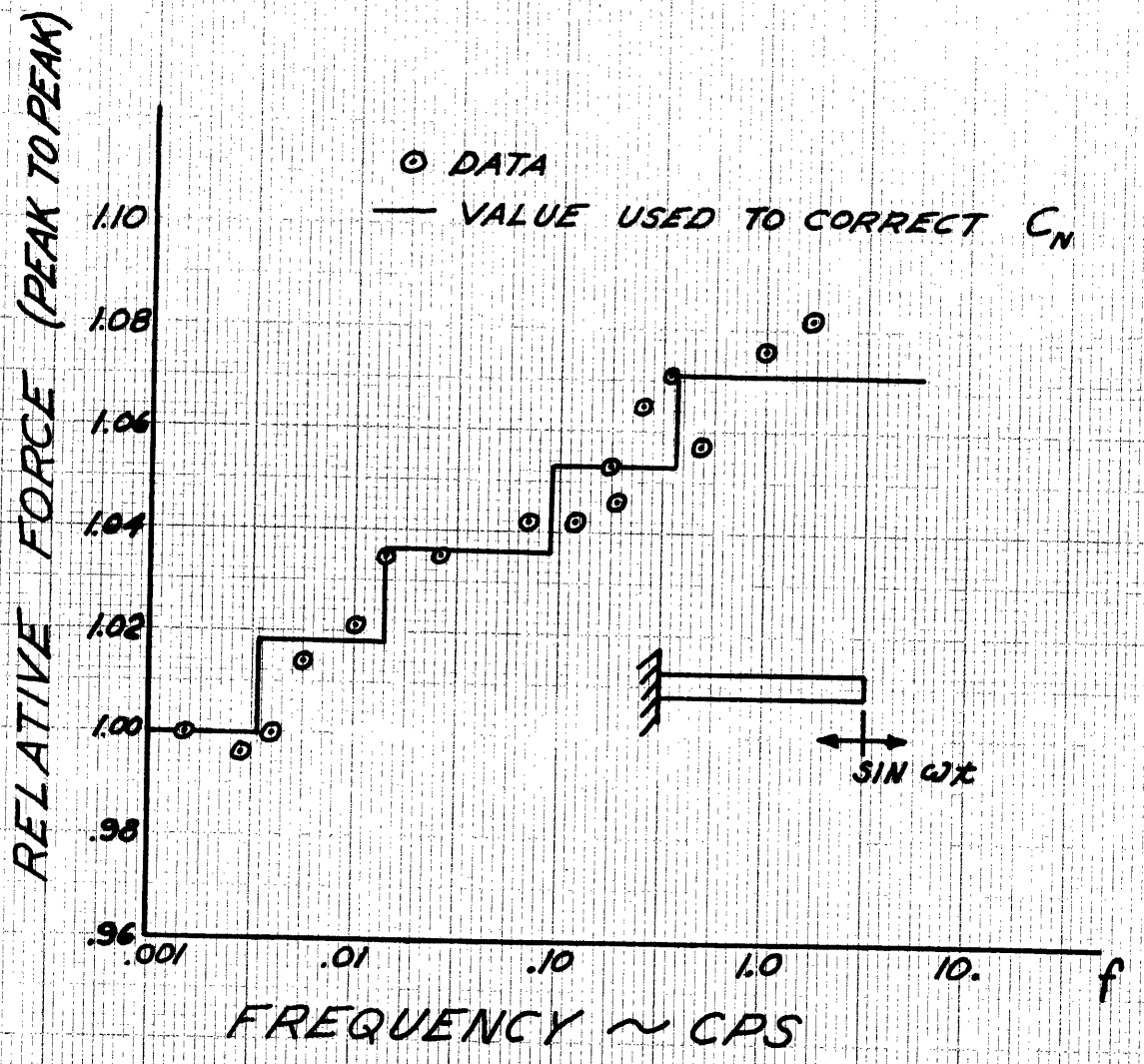

CHANGE IN STIFFNESS OF THE TUBE WALL WITH FREQUENCY

FIGURE 8

V THE FRICTION APPROXIMATION

In this section we will find the expression for τ to use in the momentum equation (4) of chapter 3. We will consider only laminar flow and neglect the entrance effects near the ends of the tube.

1. The Approximation

The large value of λ/R is again used to justify a simplifying approximation. For large λ/R the radial velocity is much less than the longitudinal velocity and one can imagine that the velocity profile would be almost the same as if the tube were rigid. Consequently, the shear stress at the wall should be almost the same as the shear stress in a rigid tube having the same flow. This idea contains the essence of the approximation.

The rigid tube problem for sinusoidal flow has been solved by Womersley and others.[1,5] From Womersley's solution for the velocity profile we can obtain the relation between the mean velocity, v, and the shear force per unit length, τ, as

$$\tau = i\pi\mu\alpha^2\left(\frac{1}{M_{10}e^{i\epsilon_{10}}} - 1\right)v$$

where

$$M_{10}e^{i\epsilon_{10}} \equiv 1 - \frac{2J_1(\alpha i^{\frac{3}{2}})}{\alpha i^{\frac{3}{2}} J_0(\alpha i^{\frac{3}{2}})}$$

Thus, τ is linearly related to v by a complex constant that is a function of α. Womersley has provided tables of the modulus, M_{10}, and the argument ε_{10}, as functions of α for α from 0 to 10 and series expansions for α greater than 10. With these tables the relation is quite easy to use. All the equations used and the results obtained in the rigid tube problem are linear. We can, therefore, simply add the Poiseuille shear force due to a steady flow component. The Poiseuille shear force is

$$\tau = 8\pi\mu v$$

If the mean velocity is given by $v = v_o (s + \sin\omega t)$ then τ will be

$$(8) \quad \tau = v_o A\left(8\mu\pi - i\alpha^2\mu\pi\left(\frac{1}{M_{10}e^{i\varepsilon_{10}}} - 1\right)\right) + i\alpha^2\mu\pi v\left(\frac{1}{M_{10}e^{i\varepsilon_{10}}} - 1\right)$$

This relation is good only for a sinusoidal flow with a steady component of arbitrary size. In a more general flow which is an arbitrary function of time the shear force depends not only on the instantaneous mean velocity, but also on the time history of the mean velocity. The phase angle introduced by the complex constant relating τ and v in equation (8) accounts for the time history dependence in the sinusoidal case.

2. A Further Approximation for the Numerical Solution

Solution by a numerical integration based on the method of characteristics would be much easier if τ were dependent only on the instantaneous value of mean velocity irrespective of the phase of the flow. For the numerical integration we will make the further approximation that τ and v are related by the real part of the constant in equation (8). That is,

$$(9) \qquad Y = n_0 a\left(8\mu\pi - \alpha^2\mu\pi \frac{\sin\epsilon_{10}}{M_{10}}\right) + \alpha^2\mu\pi n \frac{\sin\epsilon_{10}}{M_{10}}$$

At first one might think this to be a very poor approximation. Notice, however, that the approximation affects only the unsteady portion of the flow. It will be shown in chapter 6 that the unsteady friction terms serve only to determine the value of two parameters X and Y as functions of α. Y is related to the damping of the waves and X modifies the apparent wave speed. Figure 9 shows the values of 1/X and Y plotted as functions of α with and without the approximation for the numerical integration. The approximation is fairly good for high α and for very low α.

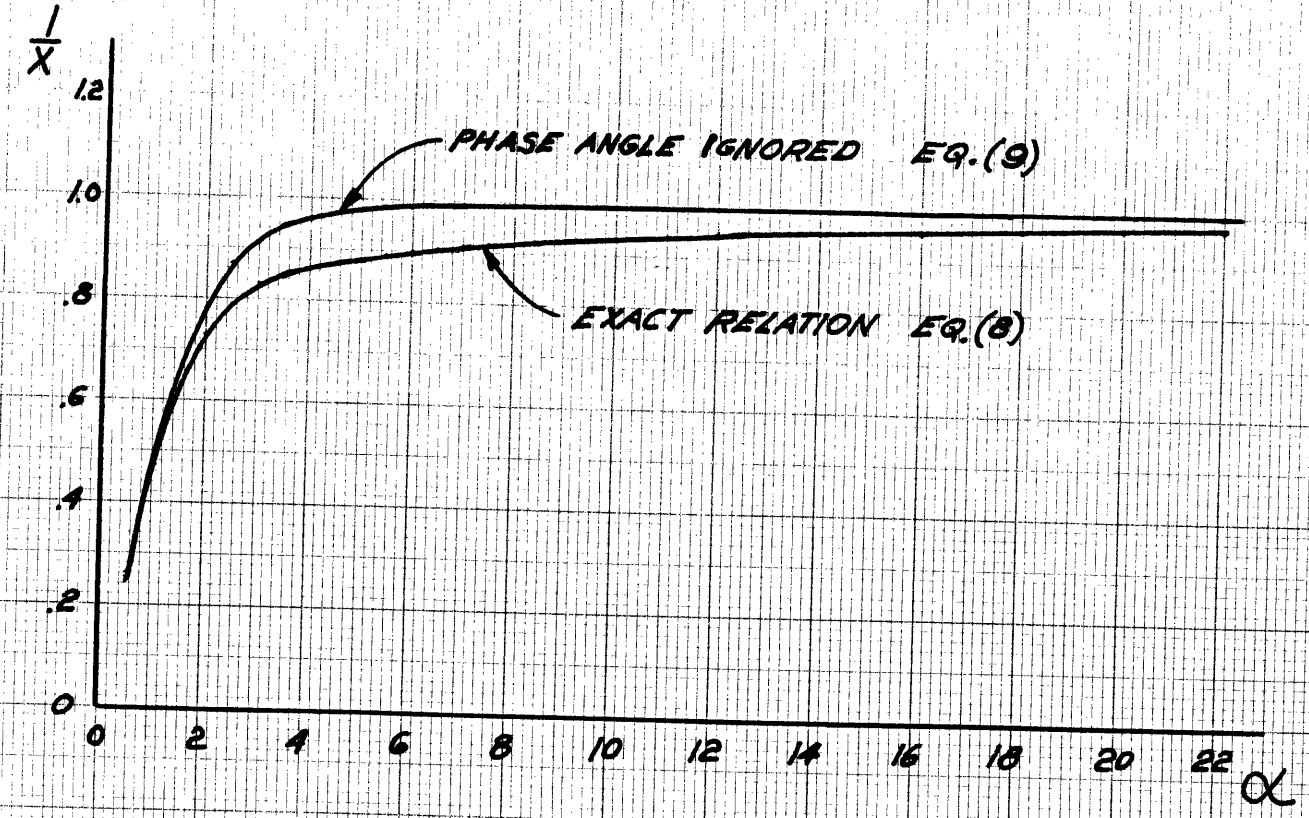

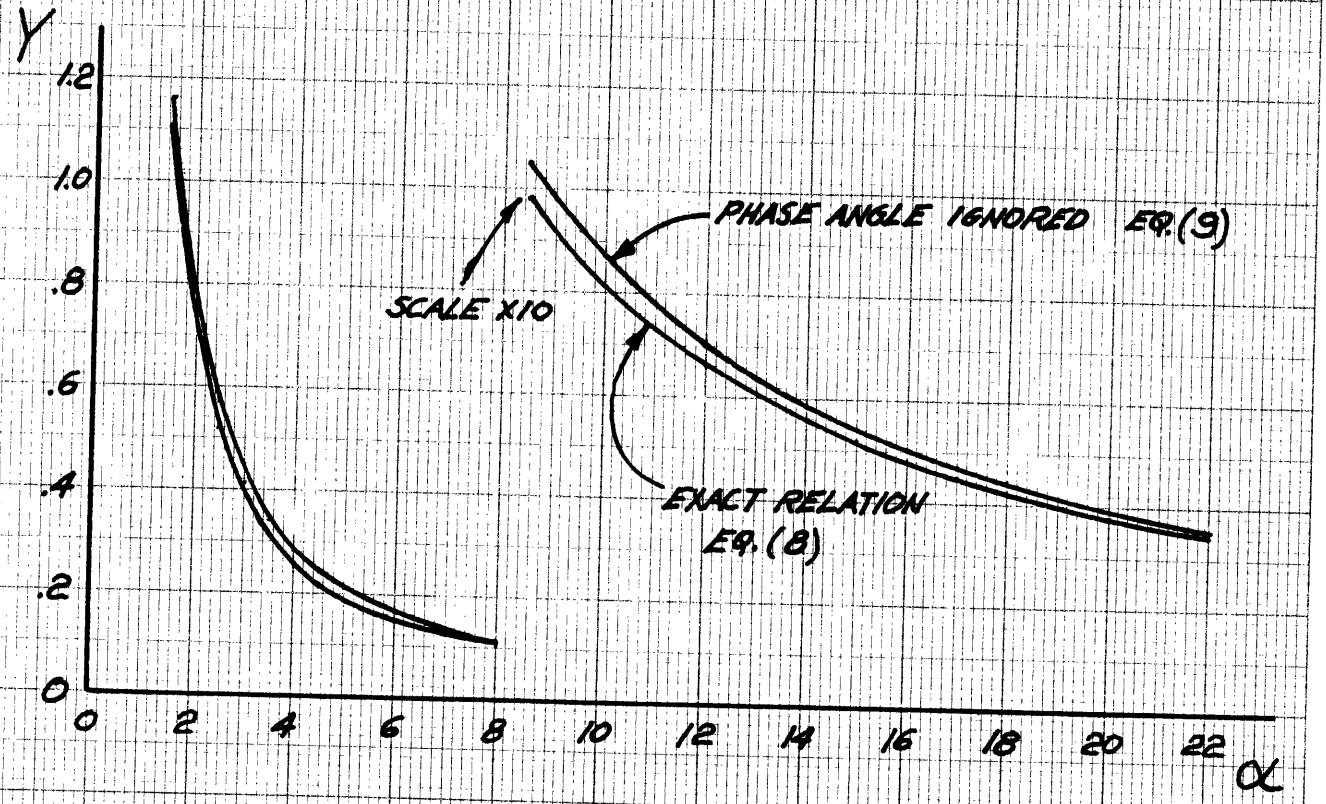

COMPARISON OF THE FRICTION RELATIONS

FIGURE 9

VI SOLUTION OF THE EQUATIONS

1. The Mathematical Problem

By collecting the previous results we obtain the following equations

$$(1) \qquad \frac{\partial(VA)}{\partial x} + \frac{\partial A}{\partial t} = 0$$

$$(10) \qquad C^2\frac{\partial A}{\partial x} + A\frac{\partial V}{\partial t} + AV\frac{\partial V}{\partial x} = -\frac{1}{\rho}\left[N_0 A\left(8\mu\pi - i\mu\pi\alpha^2\left(\frac{1}{M_0 e^{\frac{\epsilon}{2}}} - 1\right)\right) + i\mu\pi\alpha^2 V\left(\frac{1}{M_0 e^{\frac{\epsilon}{2}}} - 1\right)\right]$$

WHERE

$$(6) \qquad C^2 = C_N^2\left(2\frac{A_N}{A} - \sqrt{\frac{A_N}{A}}\right)$$

Recall that these equations are valid for sinusoidal long wavelength motions of an incompressible newtonian liquid in a long pressurized elastic tube. The flow has been assumed to be fully developed and laminar for purposes of estimating the effects of friction. The non-linear momentum term contains an approximation because the effects of a velocity profile have been ignored.

In our particular problem we prescribe the total flow $Q = Av$ at the ends of the tube. The resulting boundary conditions are

$$(11) \qquad AT \quad x = 0 \qquad AV = Q_0(1 + \epsilon \sin \omega t)$$

$$(12) \qquad AT \quad x = \ell \qquad AV = Q_0 A$$

No initial conditions are necessary because we are seeking the steady state solution where the effects of starting the motion have damped out. The problem is well defined and ready for solution.

2. An Apparent Paradox

Before proceeding with the solution, it is instructive to consider the following apparent paradox. Physically, it seems as if we could prescribe A in addition to Q by stretching the tube over a large rigid pipe. However, the equations allow only two, not four, boundary conditions. The discrepancy is resolved by noting that stretching our ideal tube over a large pipe in no way affects its area. Forces in the tube wall due to longitudinal curvature have been neglected because of the large value of λ/R. Figure 10 shows the ideal tube and an actual tube stretched over a large pipe. Note that the area of the ideal tube is not affected and that of the real tube is influenced for only a few tube radii.

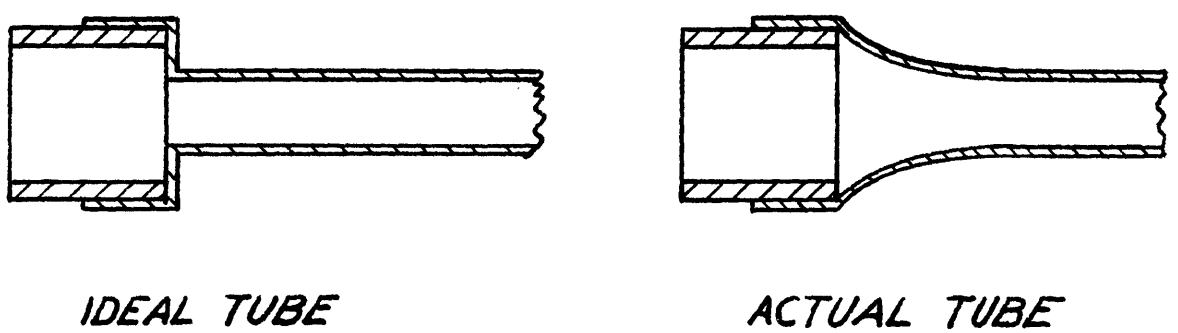

FIGURE 10

The proper way to physically prescribe the area is by prescribing the pressure. The pressure and flow cannot be prescribed simultaneously and the difficulty is resolved.

3. The Linear Frictionless Solution

Before solving the full problem, we can easily get an idea of the form of the solution by dropping the friction terms and considering a motion so small that A is almost constant and v is almost zero. For this case the equations reduce to the linear classical wave equation.

$$\frac{\partial^2 v}{\partial x^2} - \frac{1}{C_o^2}\frac{\partial^2 v}{\partial x^2} = 0 \tag{13}$$

We can identify C_o as the wave propagation speed. Note that C_o is not equal to C_N, but is the speed corresponding to the mean pressure to which the tube is inflated. With the boundary conditions given by (11) and (12) the solutions are

$$v = \frac{Q_o}{A_o}\frac{\sin\frac{\omega}{C_o}(\ell - x)}{\sin\frac{\omega \ell}{C_o}}\sin \omega t + \frac{Q_o}{A_o}\ell \tag{14}$$

$$A = A_o - \frac{Q_o}{C_o}\frac{\cos\frac{\omega}{C_o}(\ell - x)}{\sin\frac{\omega \ell}{C_o}}\cos \omega t \tag{15}$$

Thus, the solution is a standing wave which blows up at resonance when $\omega\ell/C_o$ is an integer multiple of π. We can expect that the friction terms will act to suppress the motion at resonance. The non-linear effects will be expected to distort the waves so that the motions will be not quite sinusoidal in time.

4. The Characteristic Equations

The equations (1), (10), (6) form a hyperbolic system and, therefore, possess characteristic lines. The two methods to be described for solving these equations are based on this fact. The governing equations (1), (10), (6) may be transformed to the characteristic equations by a formal mathematical procedure outlined in appendix 2. The results are

$$\frac{dx}{dt} = v \pm C \tag{16}$$

for the characteristic lines, and

$$dv = \mp C\frac{dA}{A} - \left[\frac{\nu_0 A}{A}\left(8v\pi - i\pi v\alpha^2\left(\frac{1}{M_0 e^{i\epsilon_0}} - 1\right)\right) + \frac{i\pi v\alpha^2 v}{A}\left(\frac{1}{M_0 e^{i\epsilon_0}} - 1\right)\right] dt \tag{17}$$

as the equations along the characteristics.

To simplify the problem we will form dimensionless equations by substituting the following dimensionless variables into eqs. (16) and (17).

$$\phi = \frac{A_N}{A}, \quad \phi_0 = \frac{A_N}{A_0}, \quad x' = \frac{x}{\ell}, \quad v' = \frac{v}{C_0}, \quad C_N' = \frac{C_N}{C_0}, \quad t' = \frac{tC_0}{N}$$

$$N = \frac{\omega \ell}{C_0}, \quad \epsilon = \frac{Q_0}{A_0 C_0}, \quad \eta = N\frac{A_0}{A_N} i\left(\frac{1}{M_{10} e^{i\epsilon_{10}}} - 1\right), \quad S = \frac{A_0 C_0}{A v \ell\left(8\pi - i\pi\alpha^2\left(\frac{1}{M_0 e^{i\epsilon_{10}}} - 1\right)\right)}$$

However, in agreement with the approximate relation for τ, eq. (9), we will take η and S as

$$\eta = N\frac{A_0}{A_N}\left(\frac{\sin\epsilon_{10}}{M_{10}}\right)$$

$$S = \frac{A_0 C_0}{A v \ell\left(8\pi - \pi\alpha^2\frac{\sin\epsilon_{10}}{M_{10}}\right)}$$

for use in the numerical integration method.

The variable ϕ has been chosen for convenience in the series expansion method but for consistency will also be used in the numerical integration method.

The results of the substitution are

$$\frac{dx}{dt} = v \pm C_N \phi \sqrt{2\phi^2 - 1} \tag{18}$$

$$dv = \pm 4C_N \sqrt{2\phi^2 - 1}\, d\phi - \epsilon \frac{\phi^4}{S}\, dt - v\phi^4 \eta\, dt \tag{19}$$

with the boundary conditions that

$$\text{AT } x = 0 \qquad v = \epsilon\phi^4(A + B \sin Nt) \tag{20}$$

$$\text{AT } x = 1 \qquad v = \epsilon\phi^4 A \tag{21}$$

where the primes have now been dropped and all the variables appear in their dimensionless forms.

5. The Numerical Integration Method

The numerical integration solution follows the method mentioned by Crandall[6] in which the solution at a point α is calculated by stepwise integration along the characteristics from the known values at points β and γ. (See Fig. 11.)

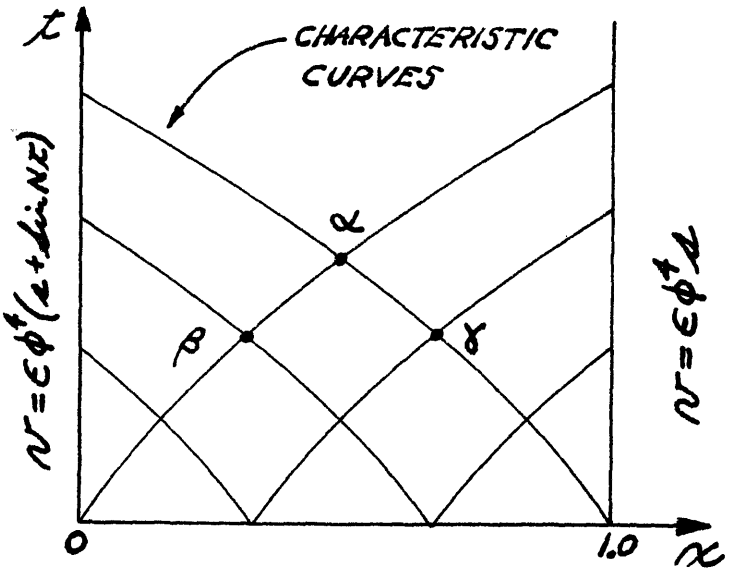

FIGURE 11

Normally this method is used for solving initial value problems rather than steady state motions. However, if we believe equations (18) through (21) to adequately represent the performance of a real tube, we would expect the solution to reach a steady state just as the motions in a real tube do. That is, we expect waves arising from the initial conditions to damp out because of the fluid friction.

The solution is started by choosing initial values for v and ϕ equal to the linear solution along the line t = o. Errors in this initial guess damp out as the computer marches forward in time and the calculation is stopped when a steady state has been reached. At equally spaced time intervals the values of v and ϕ are computed at x positions one tenth of a tube length apart by interpolation from the nearest grid points. These values are then stored for later print-out or plotting.

6. The Series Expansion Solution

The series expansion method[7] is in principle similar to the numerical integration method. The equations are integrated along the characteristic lines by analytical rather than numerical methods. The variables are expanded in a perturbation series to make the integration possible.

a) The Differential Equations

The characteristic equations in terms of the characteristic variables α and β are

$$x_\alpha = (v + c_N \phi \sqrt{2\phi^2 - 1})\, t_\alpha \tag{22}$$

$$x_\beta = (v - c_N \phi \sqrt{2\phi^2 - 1})\, t_\beta \tag{23}$$

$$v_\alpha = 4 c_N \sqrt{2\phi^2 - 1}\, \phi_\alpha - \epsilon \frac{\phi^4}{5} t_\alpha - v \phi^4 \eta t_\alpha \tag{24}$$

$$v_\beta = -4 c_N \sqrt{2\phi^2 - 1}\, \phi_\alpha - \epsilon \frac{\phi^4}{5} t_\alpha - v \phi^4 \eta t_\alpha \tag{25}$$

where the subscripts α and β denote differentiation with respect to α and β. (See appendix 2.)

The linear solution of eqs. (14) and (15) was obtained through an assumption regarding the smallness of the motion. More accurately, the driving strength as measured by ϵ was assumed small. We might then try an expansion in powers of ϵ to obtain a solution for higher values of ϵ. We will pick a form for the expansion such that when $\epsilon = 0$, there is no motion and the characteristic lines are straight with slopes given by the dimensionless wave speed corresponding to $\phi = \phi_0$. That is,

$$(26)\quad \begin{cases} \alpha = \alpha_0(\alpha,\beta) + \epsilon\alpha_1(\alpha,\beta) + \epsilon^2\alpha_2(\alpha,\beta) + \dots \\ \tau = \tau_0(\alpha,\beta) + \epsilon\tau_1(\alpha,\beta) + \epsilon^2\tau_2(\alpha,\beta) + \dots \\ \nu = 0 + \epsilon\nu_1(\alpha,\beta) + \epsilon^2\nu_2(\alpha,\beta) + \dots \\ \phi = \phi_0 + \epsilon\phi_1(\alpha,\beta) + \epsilon^2\phi_2(\alpha,\beta) + \dots \end{cases}$$

After substituting (26) into eqs. (22) through (25) and sorting the terms according to powers of ϵ, we obtain

ϵ^0 equations

$$(27)\quad \begin{cases} \alpha_{0\alpha} = \tau_{0\alpha} \\ \alpha_{0\beta} = -\tau_{0\beta} \end{cases}$$

ϵ^1 equations

$$(28)\quad \begin{cases} \nu_{1\alpha} = 4C_N\sqrt{2\phi_0^2-1}\,\phi_{1\alpha} - \dfrac{\phi_0^4}{5}\tau_{0\alpha} - \nu_1\eta\tau_{0\alpha}\phi_0^4 \\ \nu_{1\beta} = -4C_N\sqrt{2\phi_0^2-1}\,\phi_{1\beta} - \dfrac{\phi_0^4}{5}\tau_{0\beta} - \nu_1\eta\tau_{0\beta}\phi_0^4 \end{cases}$$

$$(29)\quad \begin{cases} \alpha_{1\alpha} = \nu_1\tau_{0\alpha} + C_N\tau_{0\alpha}\left(\phi_1\sqrt{2\phi_0^2-1} + \dfrac{2\phi_0^2\phi_1}{\sqrt{2\phi_0^2-1}}\right) + C_N\tau_{1\alpha}\phi_0\sqrt{2\phi_0^2-1} \\ \alpha_{1\beta} = \nu_1\tau_{0\beta} - C_N\tau_{0\beta}\left(\phi_1\sqrt{2\phi_0^2-1} + \dfrac{2\phi_0^2\phi_1}{\sqrt{2\phi_0^2-1}}\right) - C_N\tau_{1\beta}\phi_0\sqrt{2\phi_0^2-1} \end{cases}$$

ϵ^2 equations

$$(30)\quad \begin{cases} \nu_{2\alpha} = 4C_N\dfrac{2\phi_0\phi_1}{\sqrt{2\phi_0^2-1}}\phi_{1\alpha} + 4C_N\sqrt{2\phi_0^2-1}\,\phi_{2\alpha} - \frac{1}{5}\left(\phi_0^4\tau_{1\alpha} + 4\phi_0^3\phi_1\tau_{0\alpha}\right) \\ \qquad - \eta\left(\nu_2\phi_0^4\tau_{0\alpha} + \nu_1 4\phi_0^3\phi_1\tau_{0\alpha} + \nu_1\phi_0^4\tau_{1\alpha}\right) \\ \nu_{2\beta} = -4C_N\dfrac{2\phi_0\phi_1}{\sqrt{2\phi_0^2-1}}\phi_{1\beta} - 4C_N\sqrt{2\phi_0^2-1}\,\phi_{2\beta} - \frac{1}{5}\left(\phi_0^4\tau_{1\beta} + 4\phi_0^3\phi_1\tau_{0\beta}\right) \\ \qquad - \eta\left(\nu_2\phi_0^4\tau_{0\beta} + \nu_1 4\phi_0^3\phi_1\tau_{0\beta} + \nu_1\phi_0^4\tau_{1\beta}\right) \end{cases}$$

One might think that the solution should be carried to equal powers of ε and the series (26) then truncated. However, if we define the truncation error as

$$E = \frac{\text{true value - truncated value}}{\text{true value}}$$

it can be seen that the series for x and t would be more accurate than that for v because the true value of v is of order ε. Since we are interested only in changes of ϕ, the series for both ϕ and v must be carried to one order of ε beyond that for x and t. It is for this reason that only equations for v_2 and ϕ_2 are included in the ε^2 equations to be solved.

b) The Boundary Conditions

The slopes of the α and β curves in the x-t plane are determined by the characteristic equations (22) through (25). However, we are free to label these curves in any way we please. In particular, we can choose the scales and point of origin for the α,β coordinate system to simplify formulation of the boundary conditions in the α,β plane.

Notice from eqs. (22) and (23) that the dimensionless variables have been chosen so that when ε=o, (i.e., when v=o) the characteristic lines have slopes $\pm$ 1. A simple choice for the origin and scales is such that

$x = o$ is the line $\alpha = \beta$

$t = \alpha$ on the line $\alpha = \beta$

for any value of ε. (See fig. 12.)

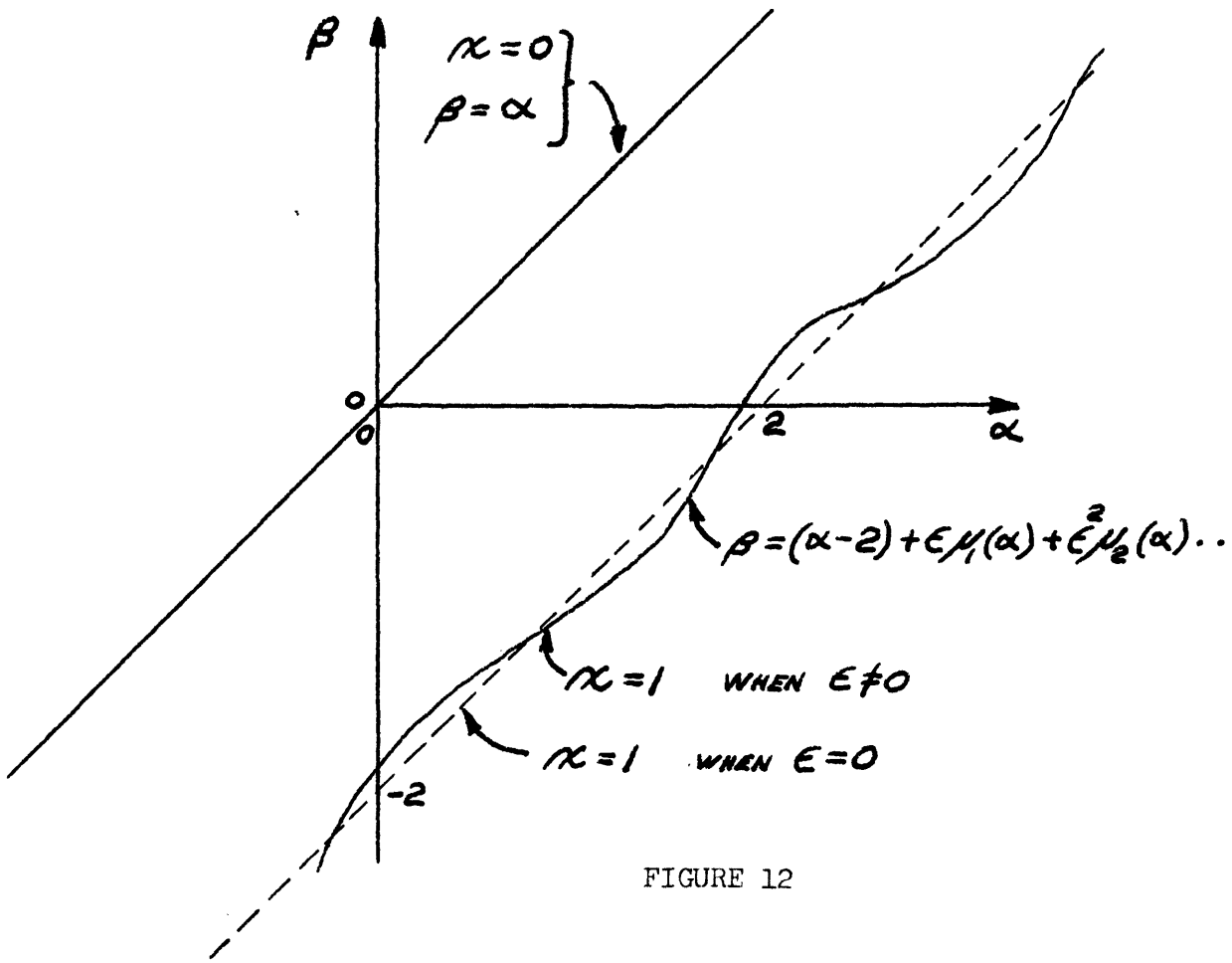

FIGURE 12

If ε=o, the line x=1 is given by β=α-2. If ε≠o, we will assume that the line x=1 warps by an amount dependent on ε. That is

$$\beta = (\alpha-2)+\epsilon\mu_1(\alpha)+\epsilon^2\mu_2(\alpha)\ldots$$

where μ_1, μ_2 are functions of α to be determined in the solution.

The lines on which the boundary conditions are to be evaluated have now been determined and we can expand the boundary conditions of eqs. (20) and (21) in powers of ε by substituting the series (26)

into (20) and (21). At $\beta=\alpha$ we have

$$\epsilon v_1 + \epsilon^2 v_2 \ldots = (\lambda + \lambda_{in} N\alpha)(\epsilon \phi_0^4 + \epsilon^2 4\phi_0^3\phi_1 \ldots)$$

$$x_0 + \epsilon x_1 + \ldots = 0$$

$$\tau_0 + \epsilon \tau_1 + \ldots = \alpha$$

We could write similar expressions at $\beta=(\alpha-2)+\epsilon\mu_1(\alpha)+\ldots$ where terms like x_1 would have to be evaluated in terms of the unknown functions μ_1, μ_2. This difficulty can be avoided by expanding terms like x_1 in a Taylor series about $\alpha-2$, thereby getting the functions μ_1, μ_2 into a position where they can be easily handled. For instance x_1 expands as

$$x_1(\alpha-2+\epsilon\mu_1+\epsilon^2\mu_2\ldots) = x_1(\alpha-2)+x_{1\beta}(\alpha-2)(\epsilon\mu_1+\ldots)+\tfrac{1}{2}x_{1\beta\beta}(\alpha-2)(\epsilon\mu_1+\ldots)^2\ldots$$

The other terms expand in a similar manner. The boundary conditions, now evaluated at $\beta=\alpha-2$, then become

$$x_0 + \epsilon(x_1 + x_{0\beta}\mu_1) + \ldots = 1$$

$$\epsilon v_1 + \epsilon^2(v_2 + \mu_1 v_{1\beta}) + \ldots = \epsilon\lambda\phi_0^4 + \epsilon^2\lambda\left(4\phi_0^3\phi_1 + (\phi_0^4)_\beta \mu_1\right) + \ldots$$

We can now sort the boundary conditions into powers of ϵ in preparation for solution as follows

<u>ϵ^0 boundary conditions</u>

at $\beta = \alpha$	at $\beta = \alpha-2$
$x_0 = 0$	$x_0 = 1$
$t_0 = \alpha$	

ε^1 boundary conditions

at $\beta = \alpha$	at $\beta = \alpha-2$
$x_1 = o$	$x_1 + \mu_1 x_{o\beta} = o$
$t_1 = o$	$v_1 = s\phi_o^4$
$v_1 = \phi_o^4(s+\sin N\alpha)$	

ε^2 boundary conditions

at $\beta = \alpha$	at $\beta = \alpha-2$
$v_2 = 4\phi_o^3\phi_1(s+\sin N\alpha)$	$v_2 + \mu_1 v_1 = 4\phi_o^3\phi_1 s$

c) The Solution

The solution begins by solving the ε^o equations and proceeding upward in powers of ε. At each step results from the previous step are available for evaluating the functions of the previous solutions appearing in the equations.

At each step the boundary conditions are given on v rather than ϕ. Since ϕ is related to v only through its derivatives, an arbitrary constant arises in the solution for ϕ. This constant is evaluated by imposing the condition that the total volume of the tube must oscillate about a mean value equal to the total volume when $\varepsilon=o$.

The solutions of the equations for the orders of ε, subject to the corresponding boundary conditions are as below.

ε^0 solution

(31) $$\chi_0 = \frac{\alpha-\beta}{2}$$

(32) $$\tau_0 = \frac{\alpha+\beta}{2}$$

These values have been substituted into the following results.

ε^1 solution

(33) $$\nu_1 = \phi_0^4 \frac{fa+gb}{a^2+b^2} \sin N\tau_0 + \phi_0^4 \frac{fb-ga}{a^2+b^2} \cos N\tau_0 + \phi_0^4 d$$

(34) $$\phi_1 = \frac{\phi_0^5}{4} \frac{ad\chi - b\epsilon X + bdY + a\epsilon Y}{a^2+b^2} \cos N\tau_0 + \frac{\phi_0^5}{4} \frac{ad\gamma - b\epsilon Y - bdX - a\epsilon X}{a^2+b^2} \sin N\tau_0 + \frac{\phi_0^5}{4} T(\chi_0 - \tfrac{1}{2})$$

These are exact solutions where

$$a \equiv \sin NX \cosh NY$$
$$b \equiv \cos NX \sinh NY$$
$$d \equiv \cos NX(1-\chi_0) \cosh NY(1-\chi_0)$$
$$\epsilon \equiv \sin NX(1-\chi_0) \sinh NY(1-\chi_0)$$
$$f \equiv \sin NX(1-\chi_0) \cosh NY(1-\chi_0)$$
$$g \equiv \cos NX(1-\chi_0) \sinh NY(1-\chi_0)$$
$$T \equiv \frac{1}{5} + \eta \phi_0^4 d = 8 \frac{Nd}{\alpha^2}$$

and X and Y are defined by

(35) $$X - iY \equiv \sqrt{1 - i\frac{\eta\phi_0^4}{N}} = \frac{\cos \frac{\epsilon_{10}}{2}}{\sqrt{M_{10}}} - i \frac{\sin \frac{\epsilon_{10}}{2}}{\sqrt{M_{10}}}$$

Notice that, as mentioned in chapter 5, the unsteady friction terms serve only to determine values for the parameters x and y of figure 9.

The solutions for x_1 and t_1 are of order ε in importance in the total solution compared to x_o and t_o. An approximation good for low friction (see fig. 9) was used to simplify the expressions for x_1 and t_1. The approximation is that X is near one and Y near zero so that the following kinds of approximation are valid

$$\text{Sinh } NY \to NY$$

$$\text{Sin } NX \to \text{Sin } N - N(1-X)\text{Cos}N$$

The corresponding approximate values for x_1 and t_1 are

$$(36)\quad x_1 = \frac{\phi_o^4}{N}\left[\frac{\left(\frac{NY(1-X^2\Phi)}{1+X} + Y\frac{1+\Phi(X+2X^2)}{(1+X)^2}\sin NX\cos NX\right)(N\pi_0\cos N\pi_0 - \sin N\pi_0) + \Phi Y \sin N\pi_0(\sin NX\cos NX - NX)}{\sin^2 NX + (NY\cos NX)^2} + Y\frac{1+\Phi(X+2X^2)}{(1+X)^2}N\pi_0\sin N\pi_0\right]\sin NT_0$$

$$-\frac{\phi_o^4}{N}\left[\frac{\sin NX\cos NX}{\sin^2 NX + (NY\cos NX)^2}\left(\frac{1-X^2\Phi}{1+X}(N\pi_0\cos N\pi_0 - \sin N\pi_0) - \Phi X\sin N\pi_0\right) + \frac{1-X^2\Phi}{1+X}N\pi_0\sin N\pi_0\right]\cos NT_0 - \frac{\phi_o^4}{2}\Phi T(\pi_0^2 - \pi_0)$$

$$(37)\quad t_1 = \frac{\phi_o^4}{N}\left[\frac{(\Phi-1)(Y\sin NX\cos NX + NXY + NX^2Y)N\pi_0\sin N\pi_0}{(1+X)^2(\sin^2 NX + (NY\cos NX)^2)} - Y\frac{1+\Phi(X+2X^2)}{(1+X)^2}\left(\sin N\pi_0 + N\pi_0\cos N\pi_0\right) + \Phi Y(\sin NX\pi_0 - NX\pi_0\cos NX\pi_0)\right]\cos NT_0$$

$$+\frac{\phi_o^4}{N}\left[\frac{(1-\Phi)X\sin NX\cos NX\, N\pi_0\sin N\pi_0}{(1+X)(\sin^2 NX + (NY\cos NX)^2)} - \frac{1-X^2\Phi}{1+X}\left(\sin N\pi_0 + N\pi_0\cos N\pi_0\right) - \Phi X\sin NX\pi_0\right]\sin NT_0 - \phi_o^4\, s\,\pi_0$$

where $\mathfrak{L} \equiv \frac{4\phi_o^2 - 1}{4(2\phi_o^2 - 1)}$

ε^2 Solutions

A glance at equations (30) and the previous solutions which must be used in equations (30) will quickly convince one that an exact solution is virtually impossible. Fortunately, high ε occurs physiologically only in regions of high α where friction is relatively unimportant. A "low friction" approximation will be used to solve equations (30).

A low friction rather than a frictionless approximation must be used in order to limit the motion at resonance. The term $\eta\phi_o^4 t_{o\alpha} v_2$ must be kept for this reason. All other friction terms will be dropped. With the low friction approximation for η that

$$\eta = \frac{2NY}{\phi_o^4}$$

equations (30) with the other friction terms omitted become

approximate ε^2 equations

$$(38)\begin{cases} v_{2\alpha} = 4\dfrac{(\phi_1^2)_\alpha}{2\phi_o^2 - 1} + \dfrac{4}{\phi_o}\phi_{2\alpha} - NY v_2 \\ v_{2\beta} = -4\dfrac{(\phi_1^2)_\beta}{2\phi_o^2 - 1} - \dfrac{4}{\phi_o}\phi_{2\beta} - NY v_2 \end{cases}$$

The boundary conditions for the ε^2 equations contain v_1 and ϕ_1. In these functions friction effects dominate and the phase of the motion shifts by 90° as resonance is approached. For an accurate approximation at resonance we must include many of the frictional terms. To simplify the problem, we will sacrifice accuracy at resonance and drop the terms that go to zero with Y, but keep the term

$$\frac{\text{SinNX}}{\text{Sin}^2\text{NX} + (\text{NY})^2\text{Cos}^2\text{NX}}$$

in the approximate form

$$\frac{\text{SinNX}}{\text{Sin}^2\text{NX} + (\text{NY})^2}$$

At resonance this term goes to zero rather than infinity and prevents the v_2, ϕ_2 terms from becoming overly important in the total solution.

The quantity μ_1 is determined by the boundary condition at $\beta=\alpha-2$ in the ϵ^1 solution. Using the same approximations as above in evaluating μ_1, we obtain approximate ϵ^2 boundary conditions as

approximate ϵ^2 boundary conditions

at $\beta = \alpha$

$$v_2 = \phi_0^8 \xi \frac{\sin NX \cos N \cos N\alpha}{\sin^2 NX + (NY)^2} + \frac{\phi_0^8}{2} \frac{\sin NX \cos N \sin 2N\alpha}{\sin^2 NX + (NY)^2}$$

at $\beta = \alpha-2$

$$v_2 = \phi_0^8 \xi \frac{\sin NX \cos N(\alpha-1)}{\sin^2 NX + (NY)^2} + \phi_0^8 \xi \frac{\sin NX \sin 2N(\alpha-1)}{2(\sin^2 NX + (NY)^2)}$$

where

$$\xi \equiv \frac{1-\Phi}{2}\left[\frac{\sin NX \cos N(\alpha-1)}{\sin^2 NX + (NY)^2}(N\cos N - \sin N) + N\sin N\right] - \Phi \frac{\sin NX \sin N \cos N}{\sin^2 NX + (NY)^2}$$

The approximate solution for v_2 and ϕ_2 are then

$$(39)\quad \nu_2 = \frac{\phi_0^8 \alpha \sin^2 NX}{(\sin^2 NX + (N\gamma)^2)^2}\left[\cos N \sin N(1-x_0) + \sin N x_0\right]\cos N\tau_0$$

$$+ \frac{\phi_0^8 \sin NX \sin 2N}{(\sin^2 NX + (N\gamma)^2)(\sin^2 2N + (N\gamma)^2)}\left[\cos N \sin 2N(1-x_0) + \xi \sin 2N x_0\right]\sin 2N\tau_0$$

$$(40)\quad \phi_2 = -\frac{\phi_0 \phi_1^2}{2\phi_0^2 - 1} + \frac{\phi_0^9 \sin NX}{4(\sin^2 NX + (N\gamma)^2)}\left[\frac{\alpha \sin NX}{\sin^2 NX + (N\gamma)^2}\left(\cos N x_0 - \right.\right.$$

$$\left.\cos N \cos N(1-x_0)\right)\sin N\tau_0 - \frac{\sin 2N}{2(\sin^2 2N + (N\gamma)^2)}\left(\xi \cos 2N x_0 - \right.$$

$$\left.\left.\cos N \cos 2N(1-x_0)\right)\cos 2N\tau_0\right] - \frac{\phi_0^9 \sin NX}{4N(\sin^2 NX + (N\gamma)^2)}\left[\frac{\alpha \sin NX \sin N}{\sin^2 NX + (N\gamma)^2}\right.$$

$$\left.\left(1 - \cos N\right) + \frac{\sin^2 2N}{4(\sin^2 2N + (N\gamma)^2)}\left(\xi - \cos N\right)\right]$$

The arbitrary constant in the ϕ_2 solution was evaluated by approximating the volume as $\int_0^{\ell} A dx_0$ rather than using the true value of $\int_0^{\ell} A dx$.

d) Validity of the Solution

The solution is now complete to one order of ε above the linear solution. We can expect it to be accurate for any value of α at low ε and for high values of α at moderate ε except near resonance. At resonance the non-linear contributions from the ε^2 terms will be in error.

VII EXPERIMENTAL APPARATUS AND MEASUREMENTS

1. The Flow Source

The flow boundary conditions of chapter 6 were provided by the system shown schematically in Fig. 13. The system is a flow source. It can produce the desired flow wave form at the tube ends independent of the pressure change across it. The dynamics of the pumping system do not enter the problem as would be the case if the pump were a peristaltic pump or some other pressure dependent source. A flow source was chosen rather than a pressure source because it could be easily built by driving a positive displacement device at constant speed with an oversize motor. The oscillating and the steady sections of the system were each driven by a 1/3 HP motor. The actual fluid power entering the tube was less than 1/40 HP.

Figure 14 shows the scotch yoke mechanism used for producing the sinusoidal piston motion. This mechanism produces a pure sine wave containing no higher harmonics. The amplitude of the piston motion is adjustable by moving the driving pin in the tee slot. The frequency is controlled by varying the rotation speed of the driver disc. Steady flows of any amplitude were provided by a Moyno positive displacement pump driven through a variable speed drive.

2. Mounting of the Tube

The elastic tube was constrained longitudinally by cementing it to a rigid table along one edge. (See fig. 15.) A very thin rubber cement was used to keep as near as possible to a line contact. The

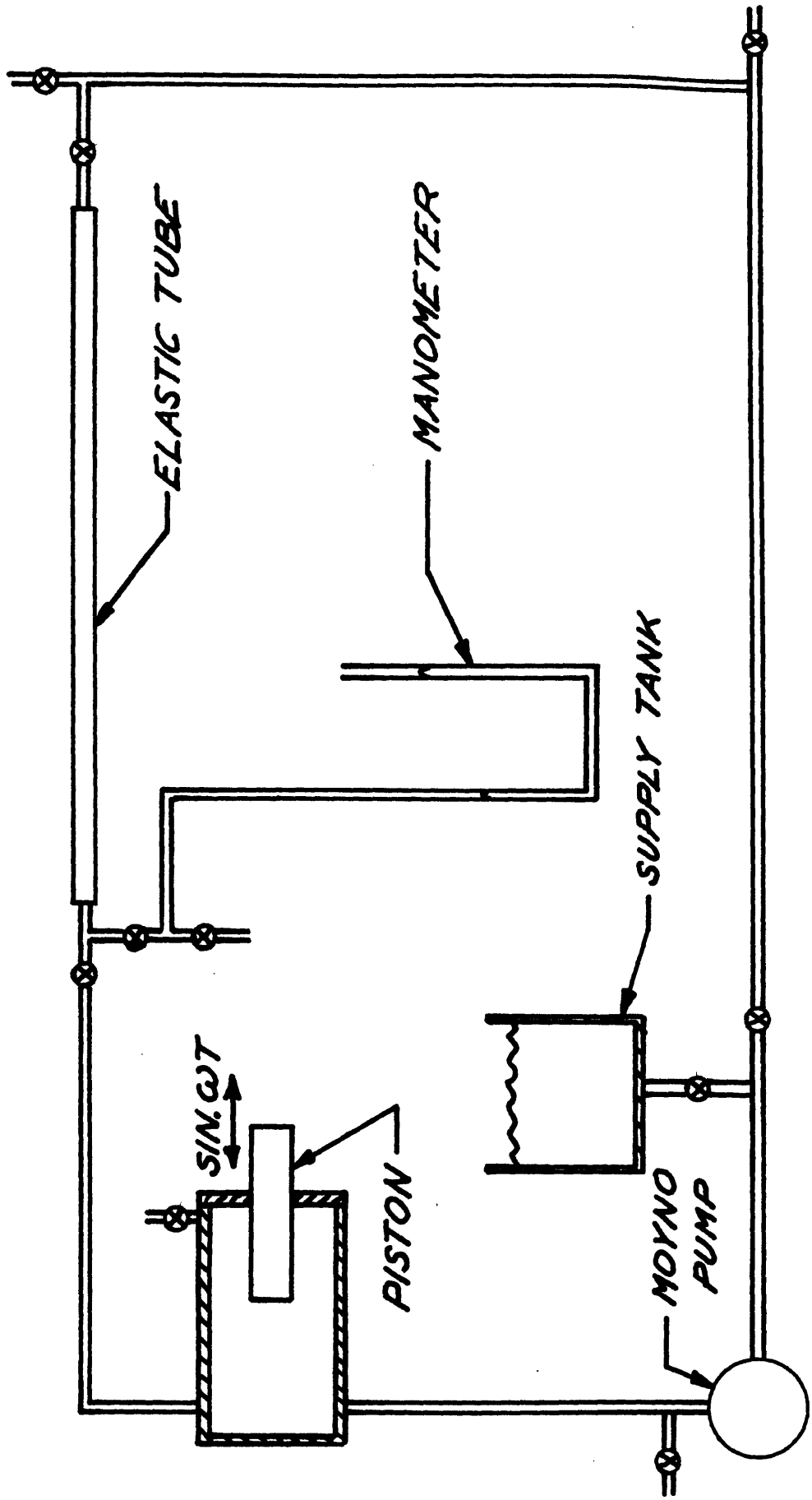

SCHEMATIC OF FLOW CIRCUIT

FIGURE 13

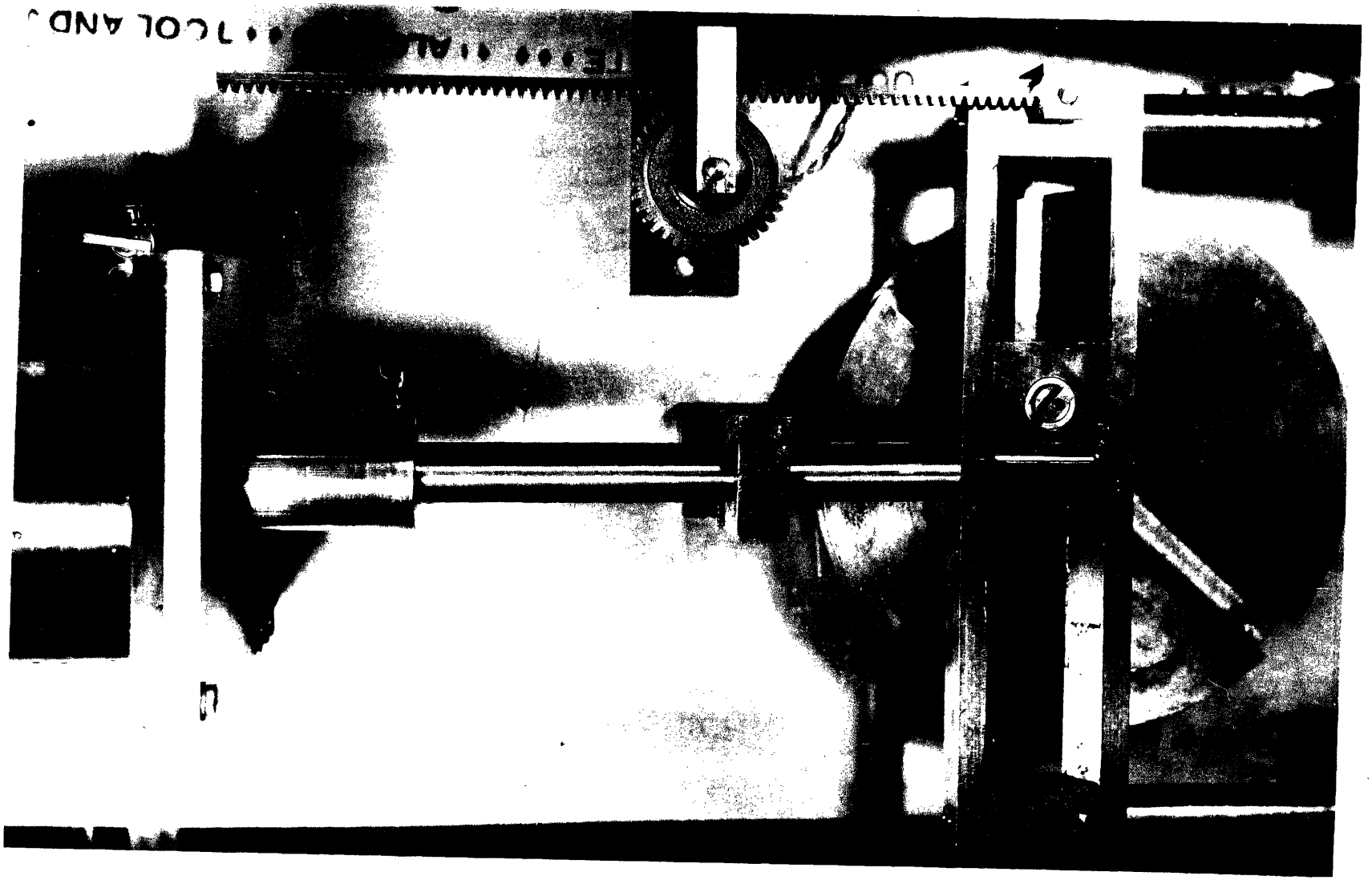

FIGURE 14

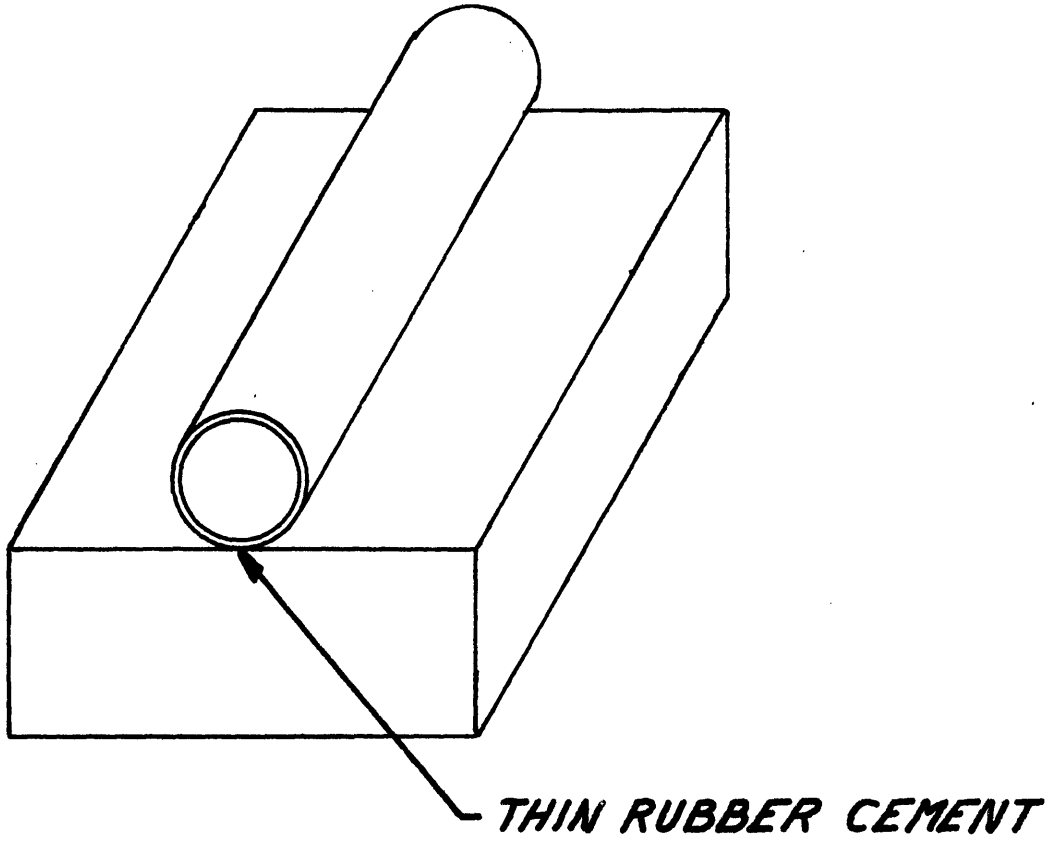

MOUNTING OF THE TUBE

FIGURE 15

tube was joined to the rigid pipes of the flow source by stretching it over the pipes and clamping it with hose clamps (fig. 16). As seen in chapter 6, this has little effect on the boundary conditions on the elastic tube.

3. Measurement of ρC_N^2

Data for the wave speed calculations of fig. 5 was obtained through the following procedure. The tube was first inflated to a large initial pressure and this value was recorded. Then a measured volume of fluid was withdrawn from the tube and the new value of pressure was recorded. The withdrawing and recording process was repeated at two-minute intervals until the pressure was reduced to zero. Usually about eight withdrawals were made. The relaxed area of the tube A_N was then measured by weighing the amount of water required to fill a short piece of the tubing of known length. The values of A at each pressure were then calculated and the results plotted in the form of fig. 5 to obtain the wave speed C_N.

4. Instrumentation

The outside diameter change as a function of time was measured with ten strain gage transducers as shown in fig. 17. The important features of the transducers are the notch for concentrating all the strain in the vicinity of the strain gages and the small bar for distributing the force over a large length of the tube. The gages were calibrated by depressing the bar with a dial indicator and adjusting the input voltage until the output was .5 volt per inch of deflection.

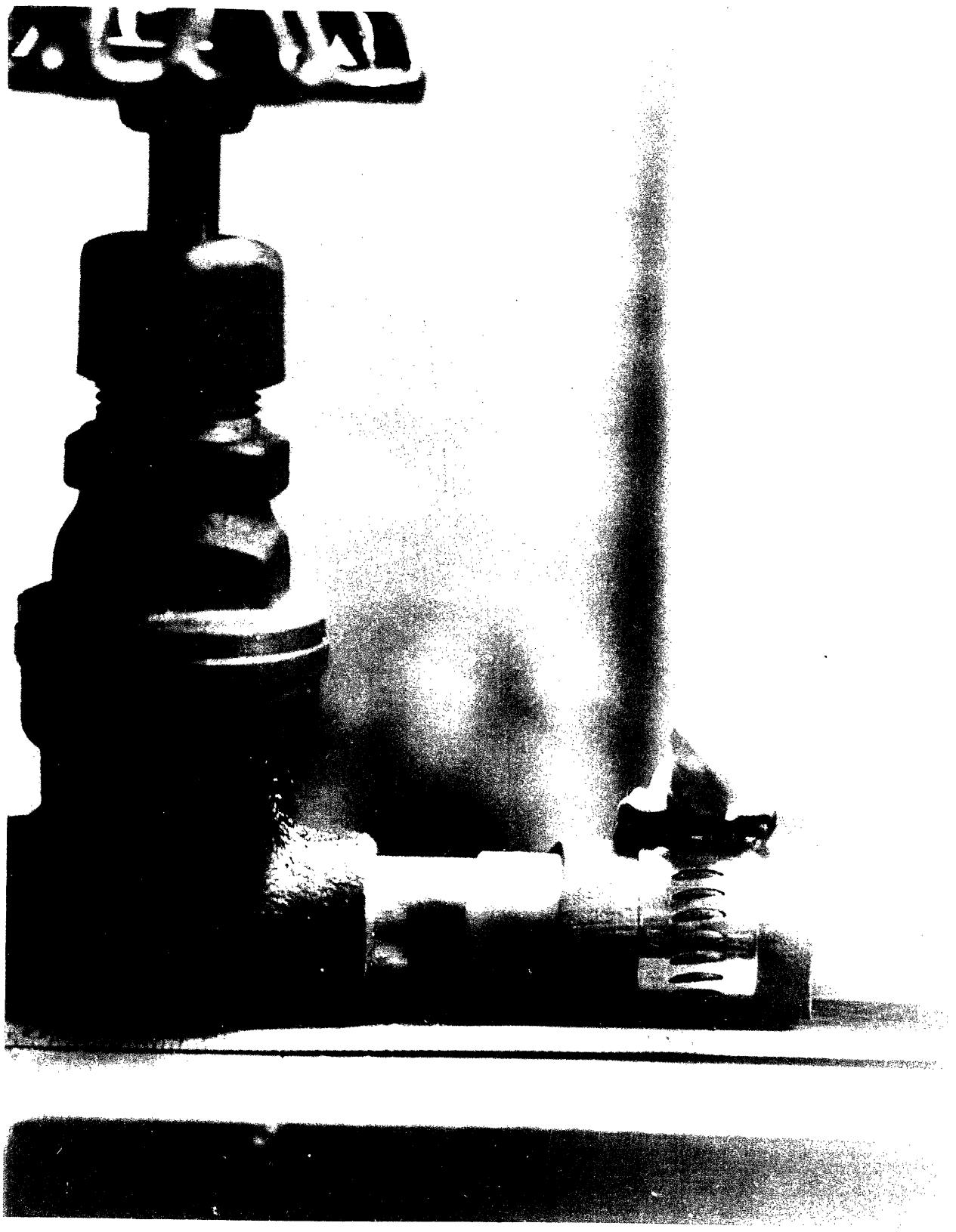

FIGURE 16

FIGURE 17

After this procedure was repeated at each transducer, a known volume of fluid was added to the tube and the change in reading from each transducer was noted. If these readings did not agree with the expected readings to within 2% the tube was rejected as being non-uniform. In an actual data run the transducers were switched, one at a time, to one channel of a two-channel strip chart recorder. The second channel was used to record piston position.

The piston position transducer is shown in fig. 14. It is simply a precision potentiometer driven by a gear and rack attached to the scotch yoke mechanism. The signal from this transducer passes through a micro switch tripped by a notch in the driver disc. Once each revolution this switch momentarily opens the circuit, producing a small sharp spike on the piston position trace. The chart paper runs at a known speed so the distance between spikes provides an accurate measure of the period of the motion.

The initial internal pressure in the tube was measured with a mercury manometer. After the measurement, the manometer was shut off and the flow was started. The manometer tube was 1.5 cm in diameter to avoid surface tension effects. The pressure measurements for the wave speed calculation were read from the manometer to $\pm$ .1 mm with a cathetometer.

5. Measurement of the Fluid Properties

Some high viscosity experiments were done using a corn syrup and water mixture. The viscosity of the mixture was measured with a viscometer made by connecting two graduate cylinders with a capillary tube. The height difference between the liquid levels in the

two cylinders can be shown to decay as $e^{-t/\tau}$ where τ is a time constant directly proportional to ν, the kinematic viscosity. Water was used to calibrate the viscometer so the viscosity ν_{CS} for the corn syrup was given by

$$\nu_{CS} = \nu_{H_2O} \frac{t_{CS}}{t_{H_2O}}$$

where t is the time for the height difference to decay to 1/4 its original value. The specific gravity of the mixture was measured with a hydrometer.

VIII RESULTS

In this chapter the experimental data is compared with results from the series expansion solution, and results from this solution are compared with results from the numerical integration solution.

1. Method of Presenting the Results

An experimental run consists of the following sequence of operations. The tube is inflated to a pressure p_o while the piston is at the center of its stroke. The pressure is recorded and the manometer and supply tank are shut off from the system. Then the zero points for each of the ten transducers are recorded on the strip-chart recorder. The flow is started and after a steady state has been reached, a few periods of the motion is recorded from each diameter transducer.

The calculation of the theoretical result begins with the experimental values for p_o, piston stroke and frequency, the amount of steady flow, and the fixed parameters of the problem like C_N and the various dimensions of the apparatus. From these values the dimensionless parameters of the theory are calculated and used in the theory to predict the motion of the outside of the tube. The predicted motion is plotted to the same scale as the experimental recording on the strip chart. Then, the experimental curves are traced through onto the theoretical plot for comparison. Figure 18 is such a plot.

Each curve in this figure shows the fluctuation of the outside diameter of the tube as a function of time at a fixed position, x, along the tube. The curve at the bottom of the figure is recorded at the tube inlet (x=o). Each higher curve is recorded one tenth of a tube length further down the tube and the top curve is recorded at the far end of the tube (x=1). The point t=o, ΔD=o is located by a small "T" in later figures. Absence of this sign indicates that zero points for the experiment were not recorded. The symbol P, for perfect, indicates that the curves being compared were almost coincident so that the difference could not be shown in the figure.

A plot like figure 18 was made for each experimental run and the plots were ordered according to degree of agreement between theory and experiment. Table 2* shows the important parameters and degree of agreement for each run. The integers in the column headed "rank" increase as the agreement becomes worse. The errors are classified A, P and S according to whether the error was mainly one of amplitude, phase, or shape of the curve. Sample plots of various ranks are given in figs. 18 through 24.

2. Effects of the Random Errors of Measurement

Random errors are introduced by inaccuracies in experimental measurements and by the 2% variations of tube properties. Because of the quantitative nature of the rank rating variations of ±5 in rank are not particularly significant. However, the random errors lead to trends that can be seen through this ±5 scatter.

* p. 63.

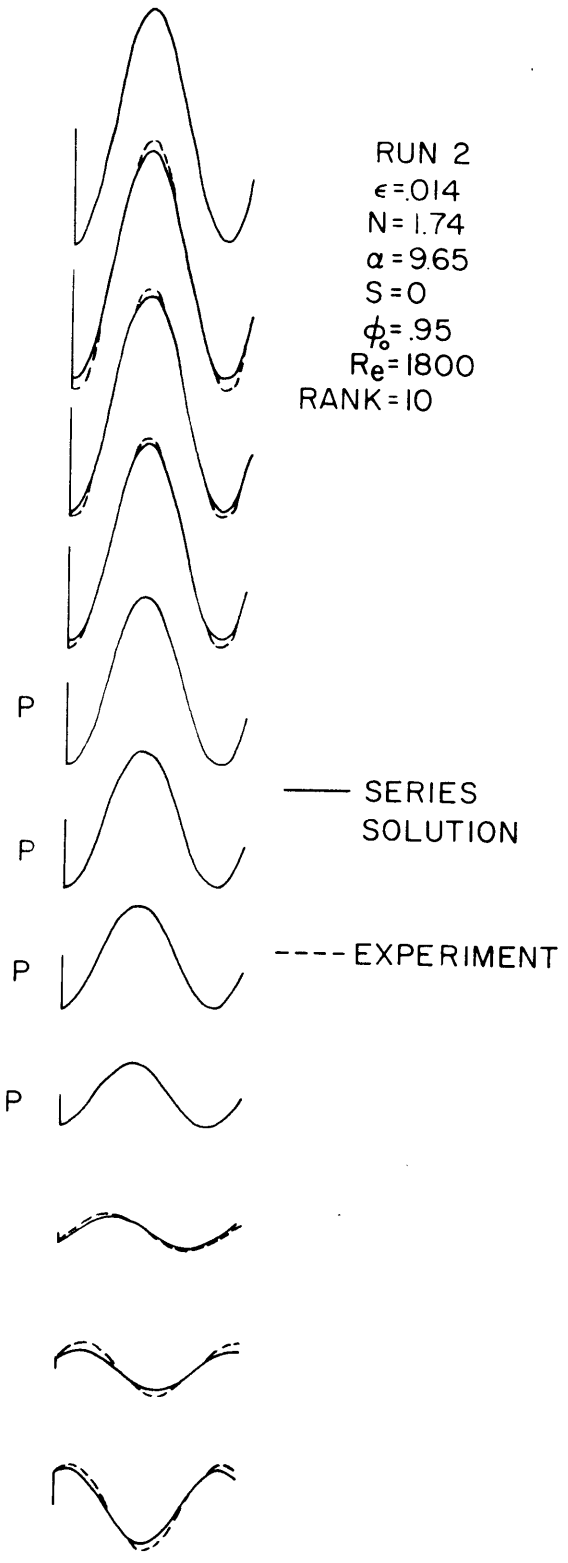

FIGURE 19

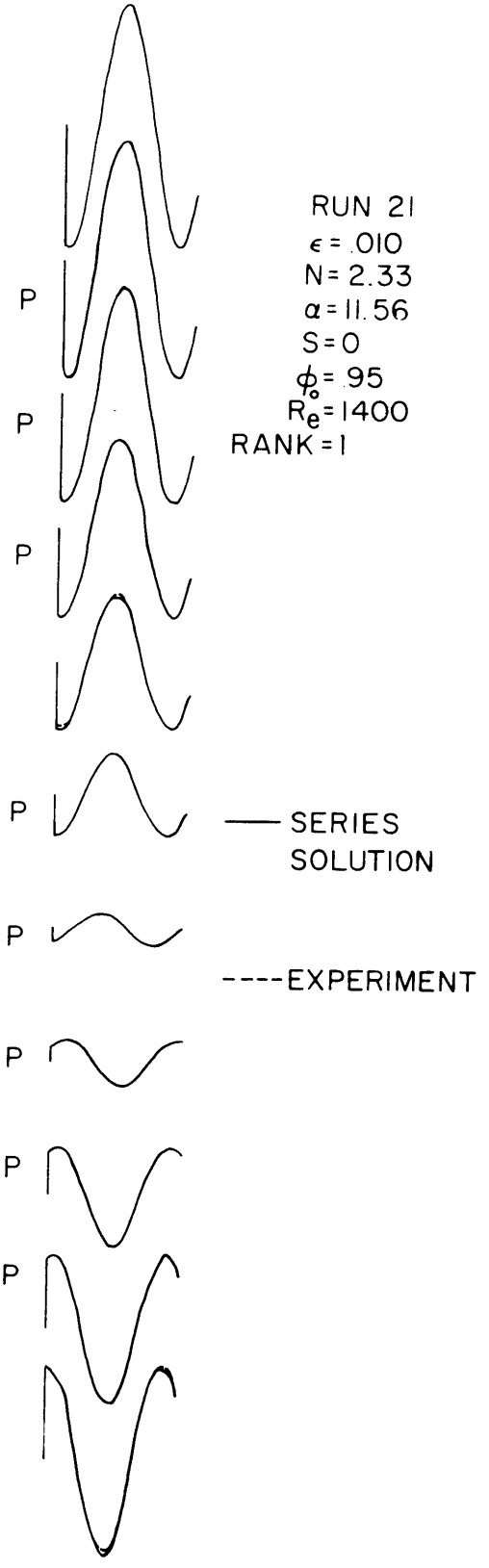

FIGURE 18

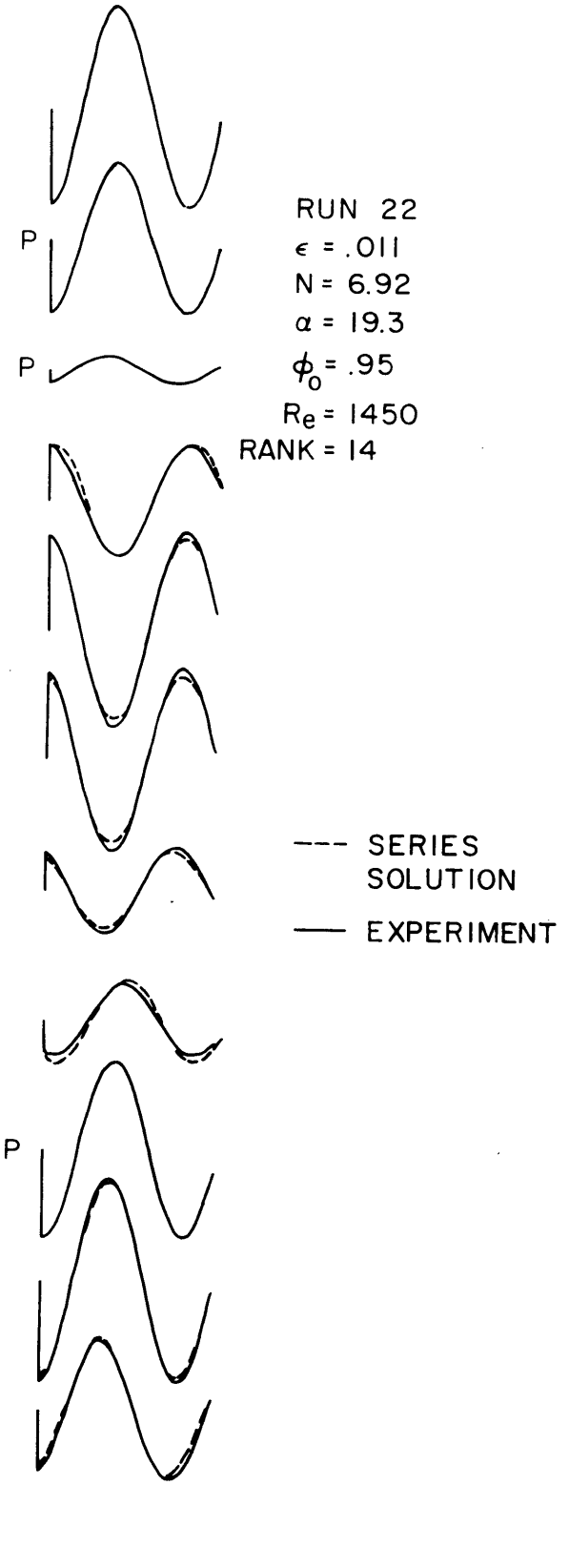

TUBE INLET
FIGURE 20

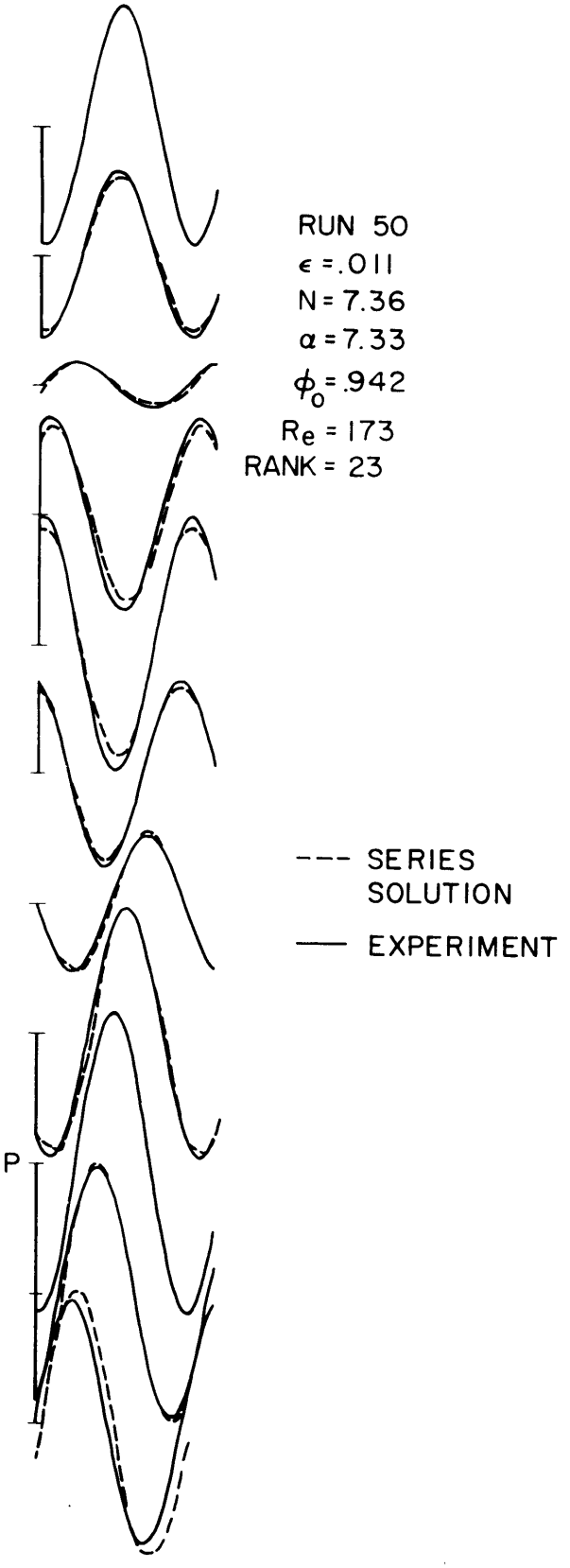

TUBE INLET
FIGURE 21

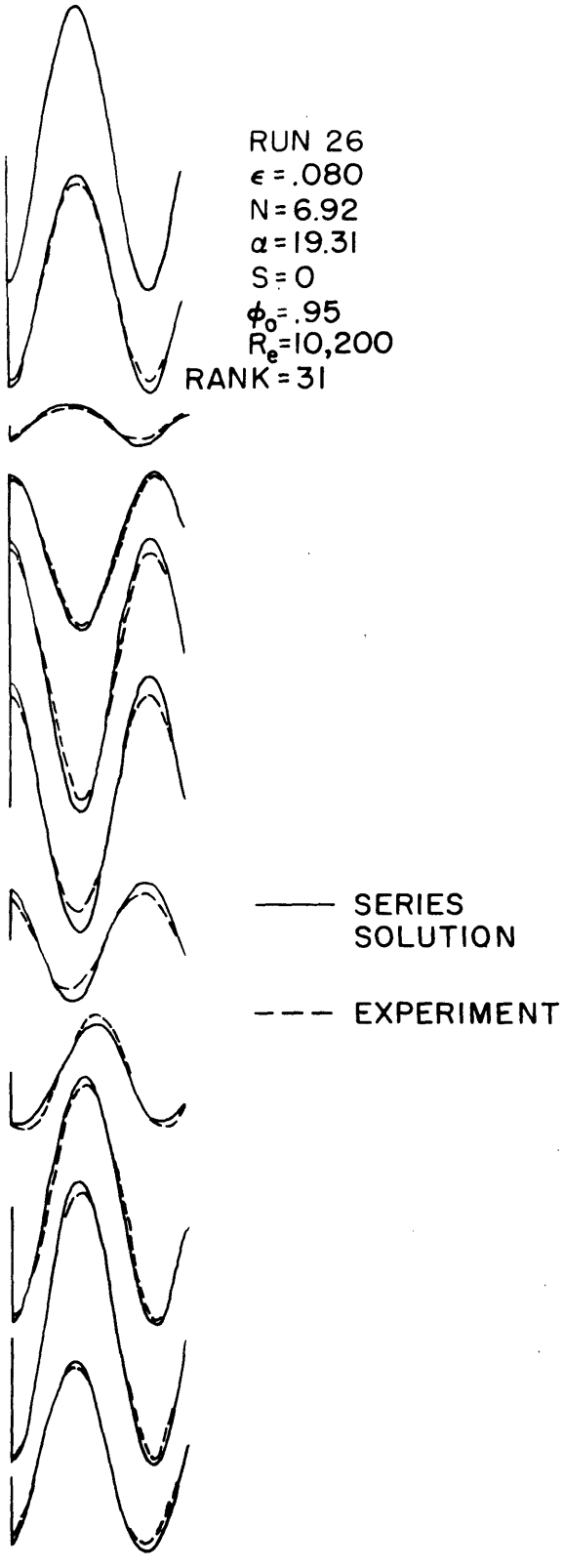

TUBE INLET
FIGURE 22

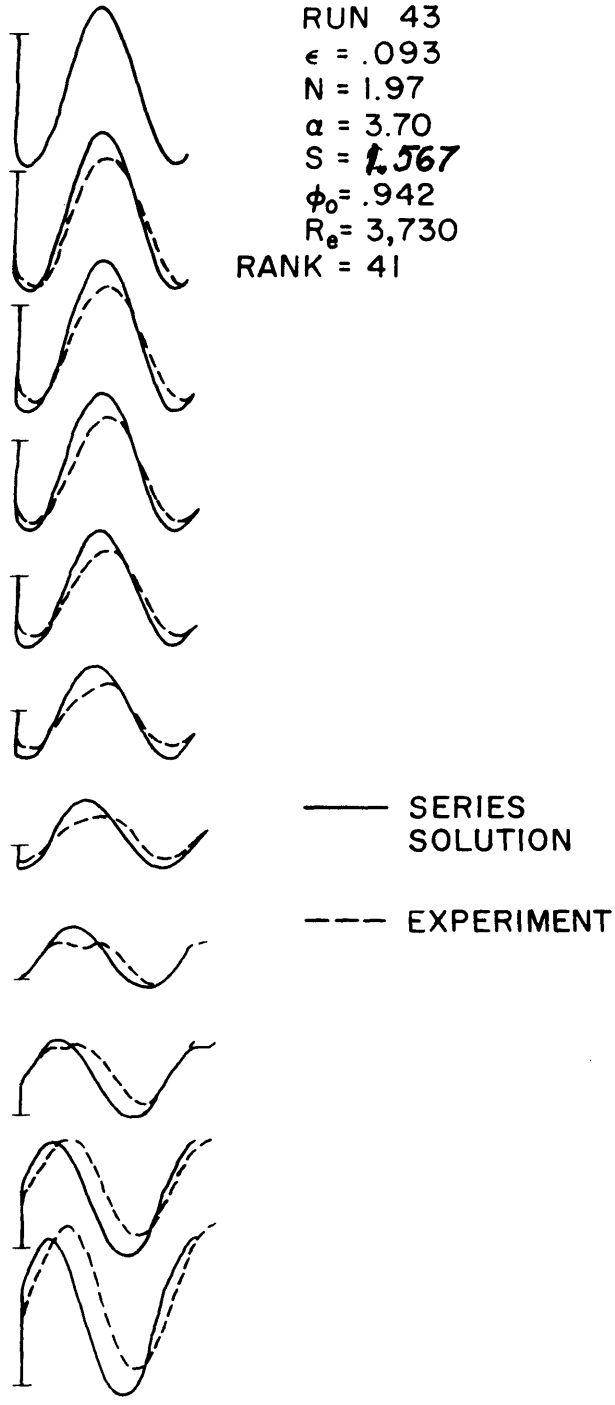

TUBE INLET
FIGURE 23

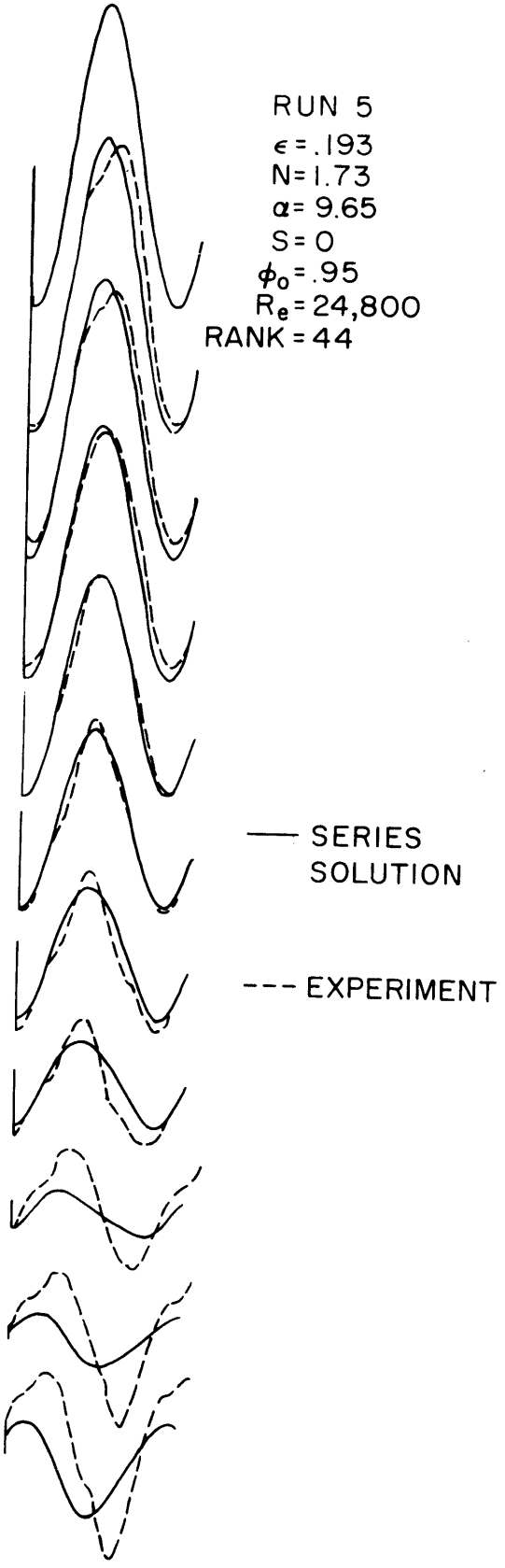

TUBE INLET
FIGURE 24

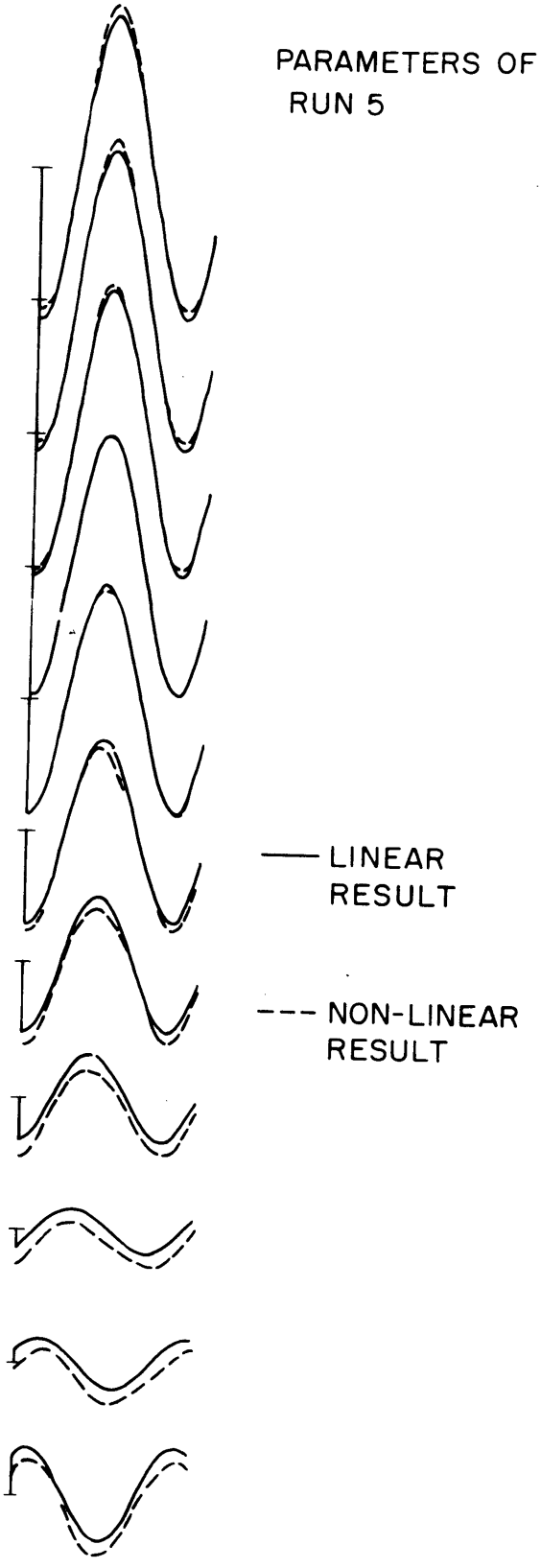

TUBE INLET
TUBE 25

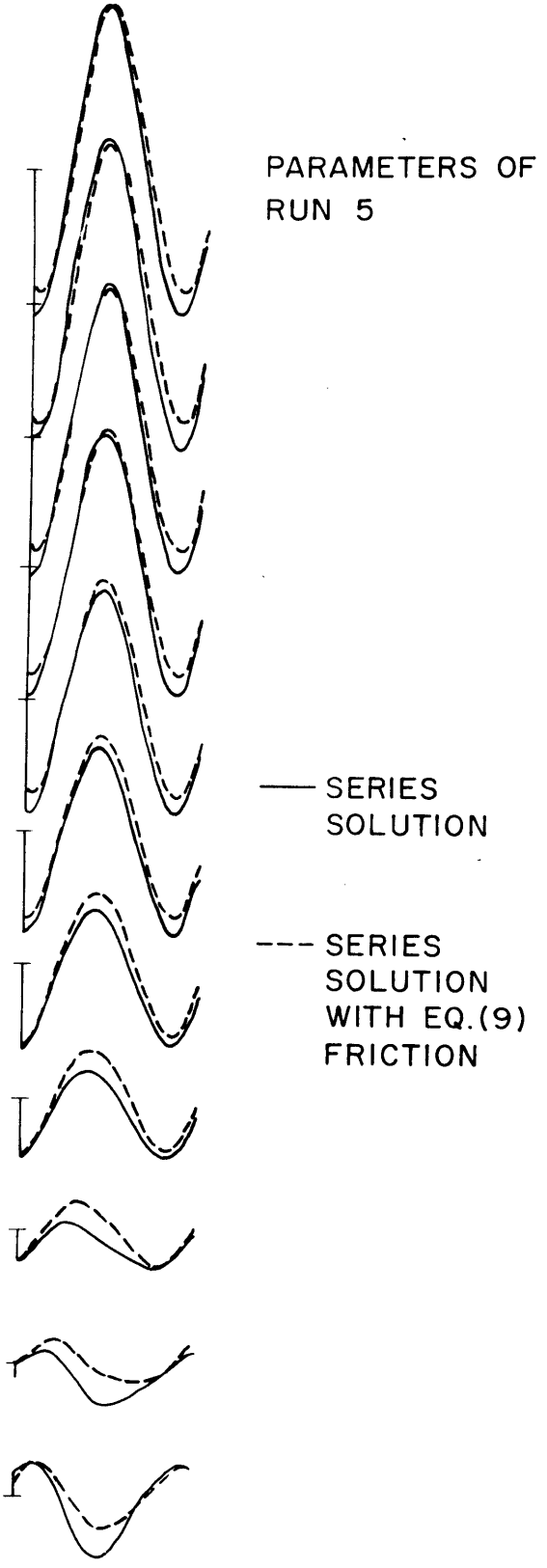

TUBE INLET
FIGURE 26

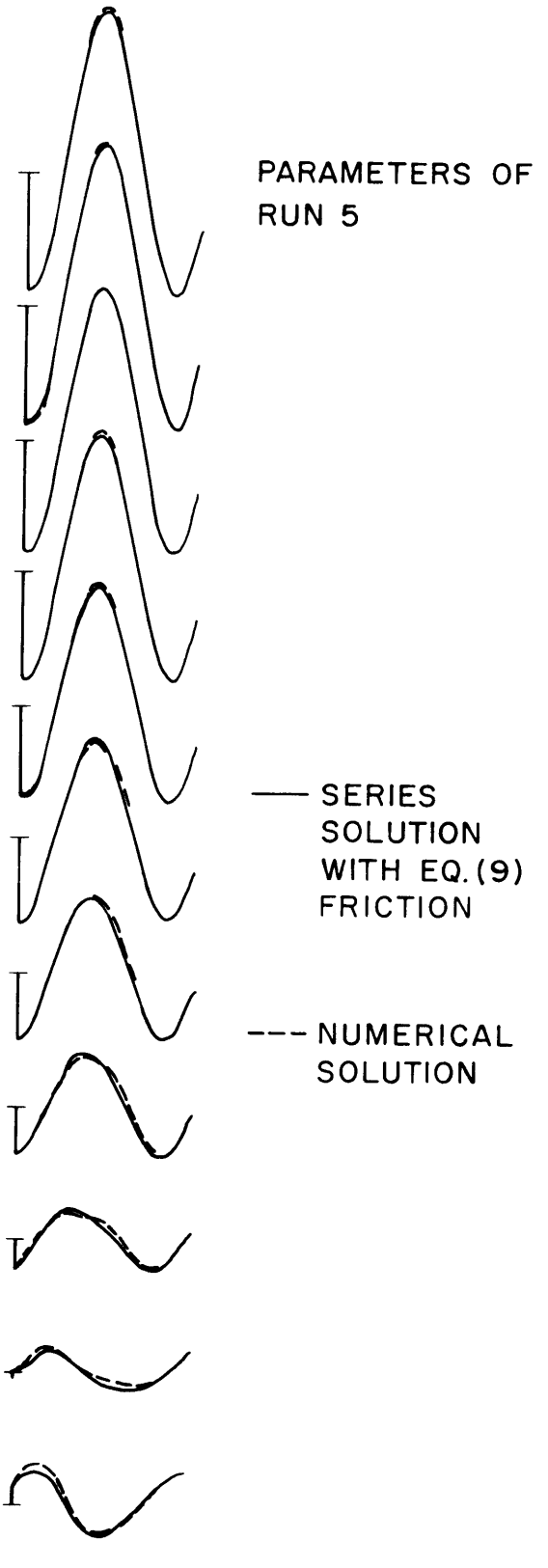

TUBE INLET
FIGURE 27

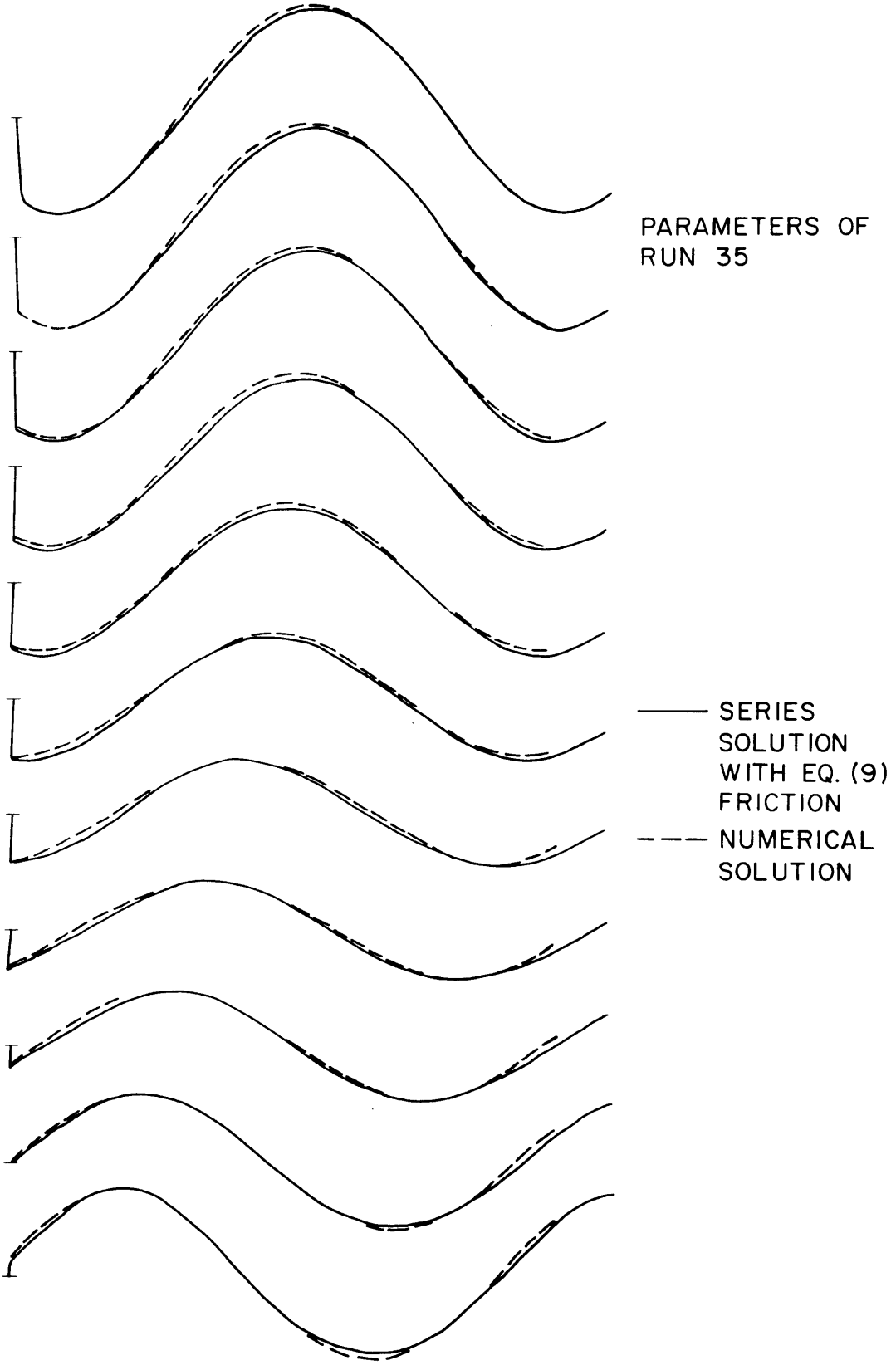

TUBE INLET
FIGURE 28

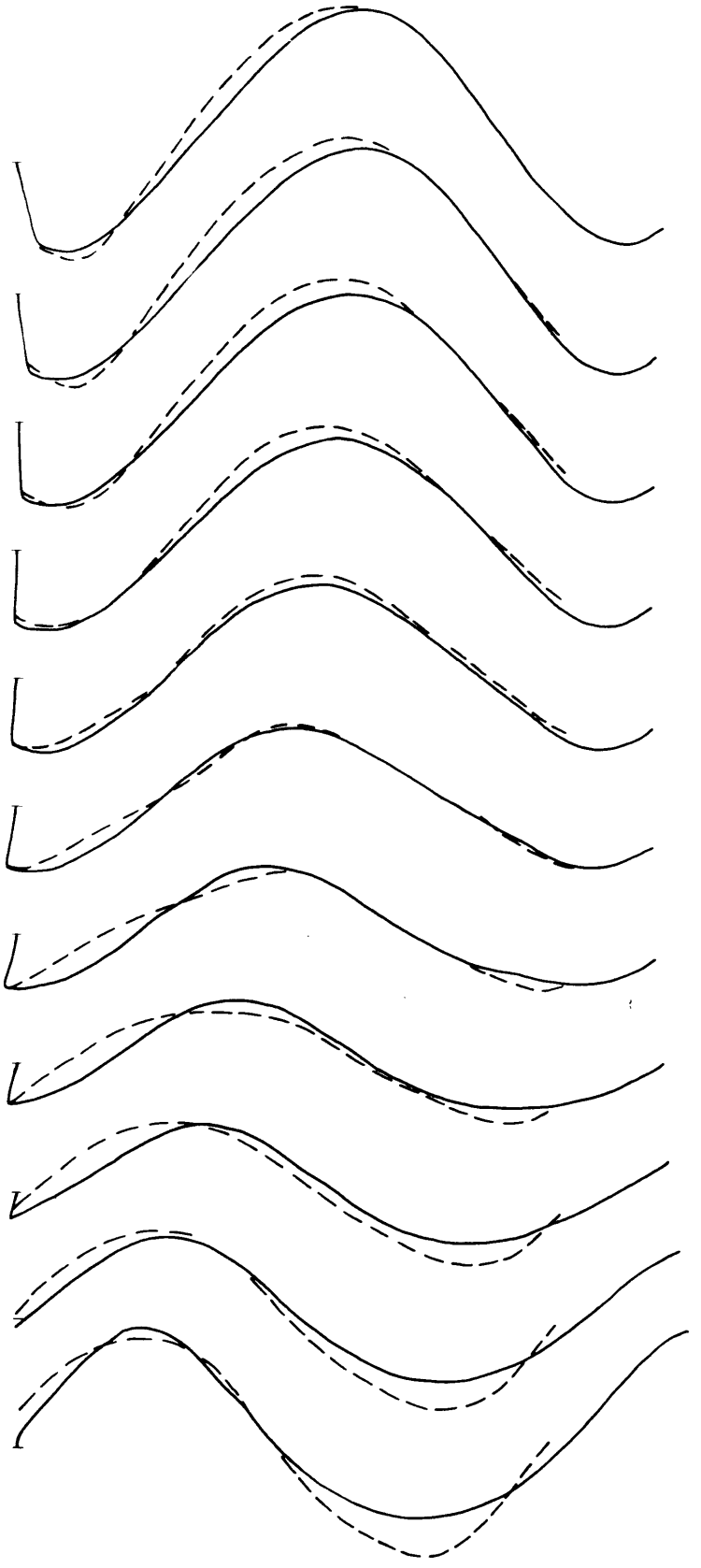

TUBE INLET
FIGURE 29

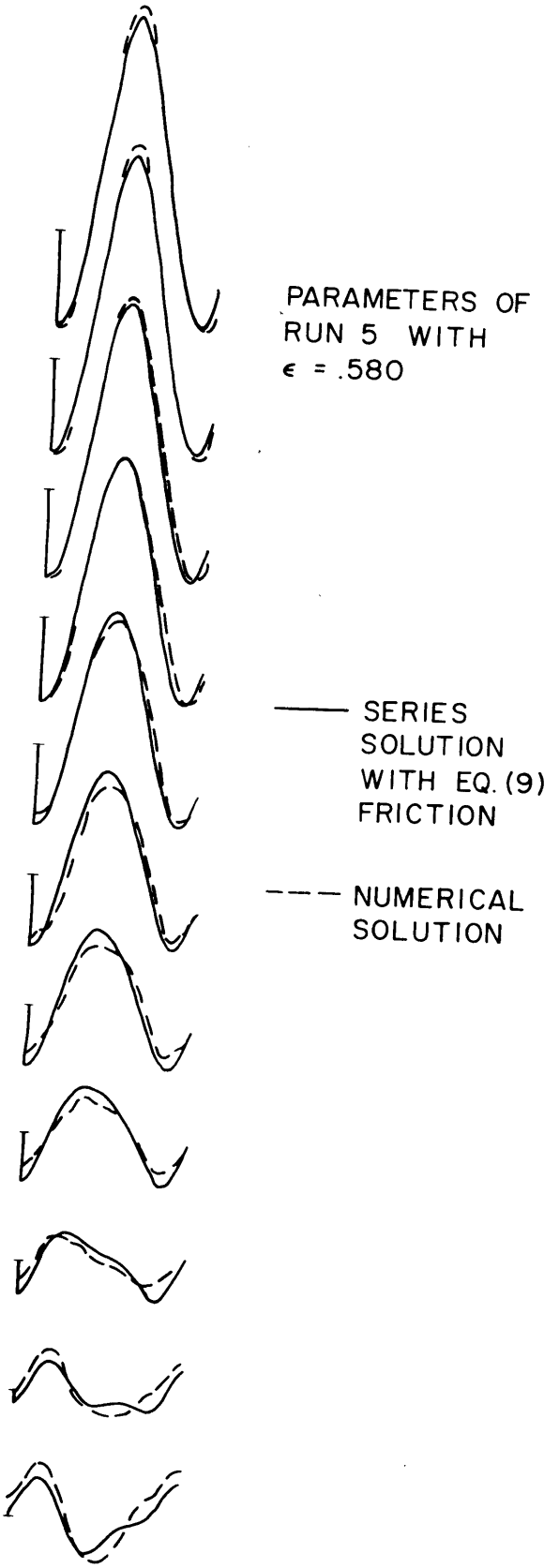
PARAMETERS OF
RUN 5 WITH
ϵ = .580
SERIES
SOLUTION
WITH EQ. (9)
FRICTION
NUMERICAL
SOLUTION
TUBE INLET

FIGURE 30

TABLE II

Run No.	ε	N	α	s	ϕ_o	R_e	Rank	Type
1	.080	1.744	9.650	0.	.950	947	12	A
2	.014	1.744	9.650	0.	.950	1,800	10	A
3	.028	1.744	9.650	0.	.950	3,600	11	A
4	.084	1.744	9.650	0.	.950	10,700	32	AS
5	.193	1.731	9.650	0.	.950	24,800	44	S
6	.015	1.815	9.890	0.	.939	1,750	16	A
7	.013	1.673	9.460	0.	.961	1,800	9	A
8	.013	1.627	9.270	0.	.971	1,900	8	A
9	.013	1.577	9.100	0.	.981	1,950	22	A
10	.084	1.735	9.660	1.586	.950	28,000	49	A
11	.084	1.744	9.650	.793	.950	19,200	48	A
12	.085	1.744	9.650	.121	.950	12,200	39	SA
13	.015	1.744	9.650	9.214	.950	18,800	47	A
14	.015	1.744	9.650	4.607	.950	10,300	46	A
15	.014	1.744	9.650	.724	.950	3,100	5	AP
16	.014	1.744	9.660	0.	.950	1,800	15	A
19	.010	.469	4.990	0.	.950	1,200	2	A
20	.010	1.144	7.840	0.	.950	1,200	3	A
21	.010	2.325	11.560	0.	.950	1,400	1	A
22	.011	6.916	19.300	0.	.950	1,450	14	SA
23	.078	.684	6.060	0.	.950	10,000	24	P
24	.077	1.409	8.700	0.	.950	9,800	34	S
25	.080	3.528	13.820	0.	.950	10,300	19	AS
26	.080	6.916	19.310	0.	.950	10,200	31	AS
27	.066	11.227	24.600	0.	.950	8,500	38	PA
31	.008	1.966	3.700	0.	.942	125	25	PA
32	.016	1.961	3.700	0.	.942	252	27	PA
33	.031	1.951	3.700	0.	.942	480	26	PA
34	.092	1.951	3.700	0.	.942	1,440	17	P
35	.166	1.951	3.700	0.	.942	2,620	42	PS
36	.017	2.046	3.820	0.	.930	248	28	PA
37	.016	1.892	3.610	0.	.953	256	6	A
38	.015	1.823	3.530	0.	.963	262	4	AP
39	.014	1.765	3.450	0.	.973	266	18	A
40	.014	1.718	3.380	0.	.982	280	37	A
41	.092	1.951	3.690	.122	.942	1,620	20	SA
42	.092	1.951	3.690	.790	.942	2,580	30	AP
43	.093	1.966	3.700	1.567	.942	3,730	41	SA
44	.016	1.961	3.700	.701	.942	428	33	AP
45	.016	1.951	3.690	4.550	.942	1,392	35	A
46	.016	1.966	3.700	9.030	.942	2,530	45	AS
47	.012	.519	1.900	0.	.942	179	13	P
48	.011	1.321	3.040	0.	.942	175	7	AP
49	.011	2.533	4.210	0.	.942	176	40	A
50	.011	7.365	7.220	0.	.942	173	23	AP
52	.084	1.518	3.270	0.	.942	1,330	29	AS
53	.084	3.811	5.180	0.	.942	1,320	21	AP
54	.079	7.436	7.250	0.	.942	1,250	36	P
55	.080	13.926	9.930	0.	.942	1,270	43	P

We will begin exploring these trends by considering the effect of errors in N and ε on the error in the area change. This error is estimated by differentiating the linear frictionless result of eq. 15.

$$\frac{\Delta(A-A_o)}{(A-A_o)_{max.}} = \left(\frac{\Delta\epsilon}{\epsilon}\right) + N\left[(1-\alpha)\sin N(1-\alpha) + \frac{\cos N\cos N(1-\alpha)}{\sin N}\right]\left(\frac{\Delta N}{N}\right)$$

Notice that errors in area due to errors in N become important for large N and for values of N near resonance. In fact, for low Reynolds number runs that are similar except for N, (19-22, 47-50, 52-55), the values of rank increase with N within the expected ± 5 scatter. An exception is #49 which is the only run near resonance and has the expected larger rank.

By Comparing eq. (34) with the frictionless result (i.e., eq. (34) with X=1 and Y=o) we see that as Y goes to zero, the phase angle between the two solutions goes to zero. The phase angle depends on N in addition to Y. Errors in phase angle, therefore, arise from errors in N or Y and are most apparent for large Y. Note that the runs of high α, (1-27) have fewer errors in phase than the runs of low α, (30-55), as expected.

3. A Systematic Error

Table II shows another type of error that seems to be associated with large values of Reynolds number. The Reynolds number in Table II is based on the maximum fluid velocity at the inlet of the tube. There are two possible type of errors than can arise when the

Reynolds number is large. Both are connected with the friction approximation. For calculating the wall shear stress the flow was assumed laminar and fully developed. Both these conditions depend on the Reynolds number being small. For a steady flow in a rigid tube about Re/5 tube diameters are required to reach fully developed flow, and turbulent flow occurs at Re greater than 2200. These values are probably different for an oscillating flow, but can be used as a rough guide. For the tube used the steady flow entry length is one half the tube length at about Re = 2200. Therefore it is difficult to separate errors due to entry length from errors due to turbulence, and this separation has not been attempted.

There are two effects of having turbulent rather than laminar flow. The shear stress at the wall is larger, and the shear stress is not linearly related to the mean velocity. Because of the pressure drop due to the shear stress at the wall, a steady flow produces a taper in the tube wall. A turbulent flow should produce more taper than one would predict on the basis of a laminar flow. Figure 31 shows the ratio of the actual angle of taper to that predicted by the series solution, as a function of Reynolds number. The taper is greater for high Reynolds numbers as expected.

There is a second observable phenomena due to increased friction forces. Comparison of the frictionless case with the viscous case shows that the motion at the nodes of the standing wave increases as the friction goes up. The physical explanation is that the reflected wave damps out before it can return and cancel the incident wave at the

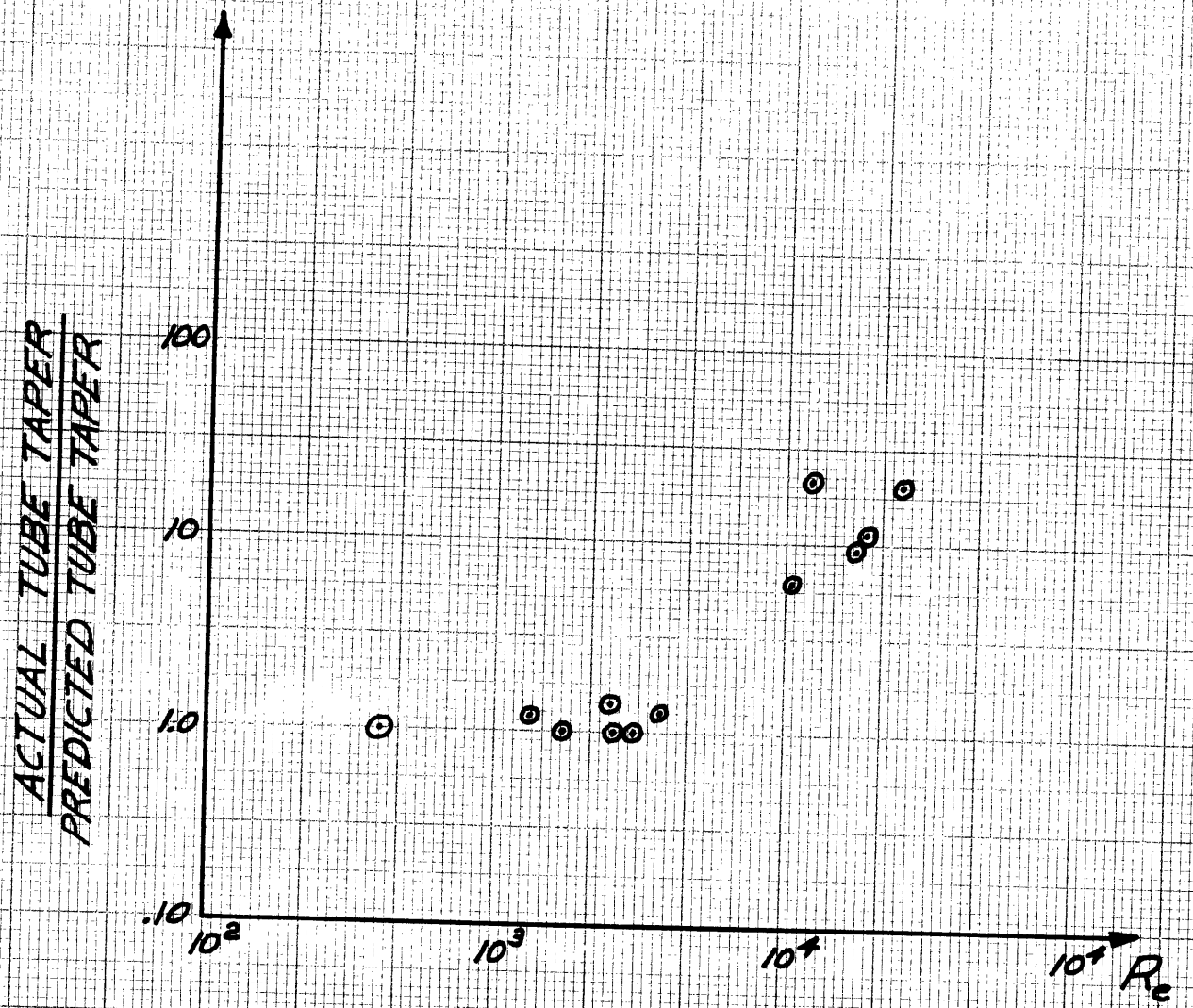

EFFECT OF REYNOLDS NUMBER ON TAPER INDUCED BY A STEADY FLOW

FIGURE 31

nodes. If we plot the amplitude of the sinusoidal portion of the diameter change as a function of distance along the tube for a low and a high Reynolds number run as in fig. 32, we see that the node of the high Reynolds number is filled in as if the steady turbulent flow had increased the friction for the oscillating component.

Figure 24 shows the data and calculated results for run number 5. A possible explanation for the large error and odd shape of the experimental curve lies in the large Reynolds number. Since the flow at the far end of the tube goes to zero, the Reynolds number must decrease between the node and the end. The highest shear stresses will occur in the neighborhood of the node. If an excess resistance is placed at the node one would expect an excess pressure amplitude before the node to force the required fluid through. Further, if this resistance were to vary with the flow, a non-sinusoidal pressure curve could result.

The best runs are all runs of low ε, but these are also runs of low Reynolds number. The question is whether the error in the high ε runs is due to Reynolds number effects or whether it represents a deficiency in the series solution. Several of the higher ε runs, (25, 41,53), show good agreement and in fact, deviations from sinusoidal form are accurately predicted for most high ε runs. However, the deviations from the linear theory are overshadowed in magnitude by errors in ε and N and by the sensitivity of the theory to the friction approximation. Several computational experiments will be used to illustrate this point.

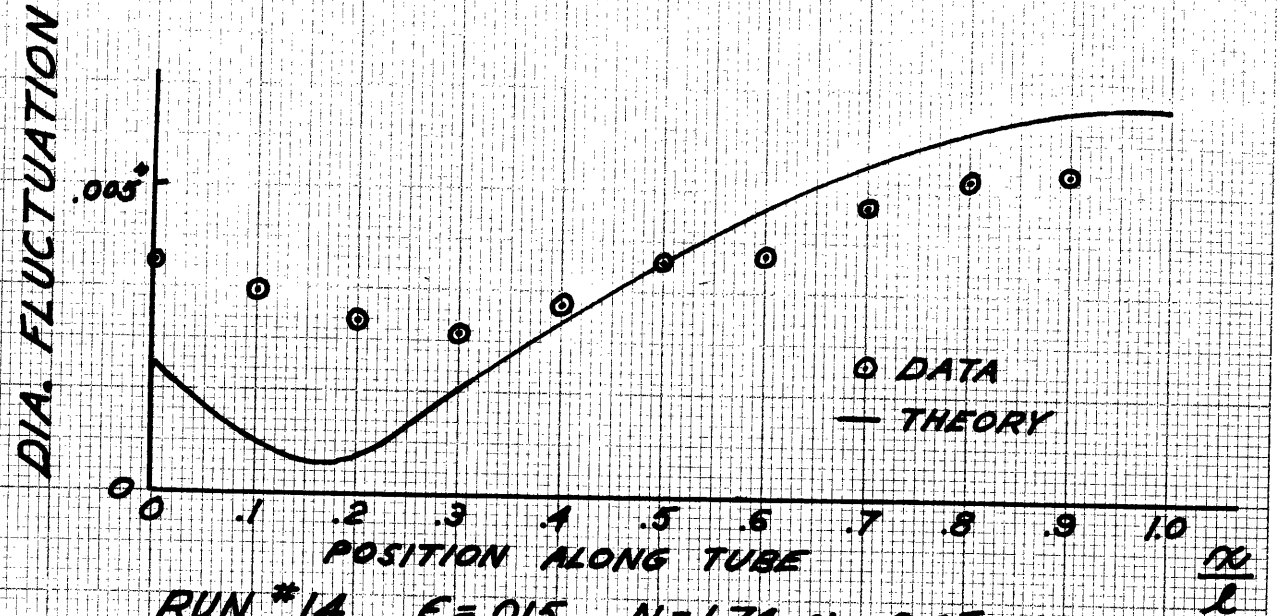

RUN #14 $\epsilon = .015$ $N = 1.74$ $\alpha = 9.65$
$S = 4.60$ $R_e = 10,360$

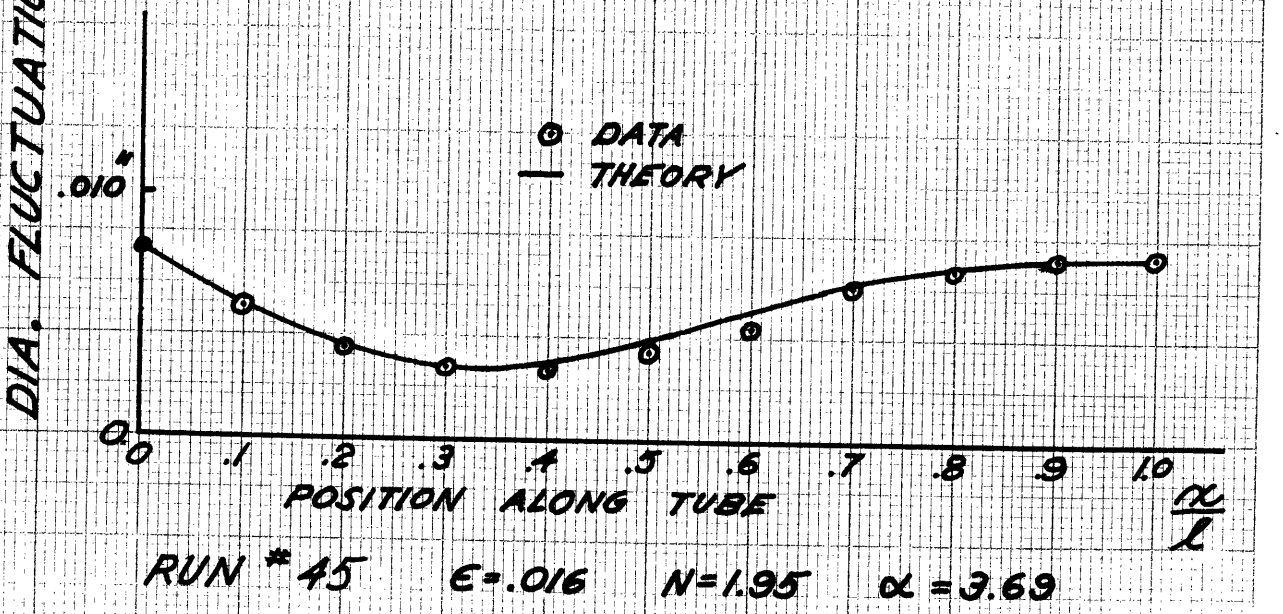

RUN #45 $\epsilon = .016$ $N = 1.95$ $\alpha = 3.69$
$S = 4.55$ $R_e = 1392$

EFFECT OF REYNOLDS NUMBER ON MOTION AT THE NODES

FIGURE 32

4. Some Computational Experiments

We will begin by comparing the calculated result for run #5 with a calculated result in which the piston stroke was reduced by a factor of 100 and the scale factor for the recorder was increased by 100. By this procedure the value of ε is cut by a factor of 100 and the linear solution is obtained. Figure 25 shows the result of this calculation. Notice that the shapes of some of the curves are quite different but that the percentage difference based on the maximum motion is quite small.

For a second computational experiment we will compare the results of two calculations using the parameters of run #5 but with two different friction approximations, one given by equation (8), the exact rigid pipe solution and one by equation (9), the approximate result used in the numerical integration method. The two solutions were obtained simply by substituting the appropriate values for X and Y from fig. 9 into the series expansion solution. Notice that the difference between these two results is greater than the difference between the linear and non-linear cases in the previous comparison of fig. 25. (See fig. 26.)

As a third computational experiment we compare results from the series expansion solution again using the friction approximation of equation (9) with results from the numerical integration solution. For low values of ε both solutions contain the same approximations. As a result, the two solutions should be identical for low ε runs and, in fact, they are. The results from higher ε computations

using the parameters for runs 5 and 35 are shown in figs. 27 and 28. Recall from chapter 6 that the terms in the series solution of higher order in ε were computed using a low friction approximation. No such approximation was used in the numerical integration solution. For this reason fig. 27 with $\alpha = 9.65$ shows better agreement than fig. 28 where the friction is greater, ($\alpha = 3.70$).

If the computations using the parameters of #5 and #35 are repeated as above but with ε increased by a factor of 3, the curves of figs 29 and 30 result. At these large values of ε the series solution is beginning to fail because of its truncation errors. The numerical integration solution, on the other hand, contains no such errors and continues to give a correct solution. The discrepancies in figs. 29 and 30 are a result of this fact.

These computational experiments have demonstrated that the series solution properly accounts for the non-linear terms of equations (1,10,6) for moderate ε and high α (physiological range), and that the calculation is quite sensitive to friction. The non-linear terms of equations (1,10,6) are accurate except for the $\bar{v}^2 = \overline{v^2}$ approximation discussed in appendix I. It is quite possible, therefore, that the large errors in the high Reynolds number runs are due to increased shear stress at the tube wall arising from turbulence or entry length effects.

IX SUMMARY AND CONCLUSIONS

In this section the new techniques, procedures and results presented in the previous chapters will be summarized, and some ideas about future work will be presented.

1. New Experimental Techniques

There are usually several possible methods for doing the same experimental work. Some of the new techniques used and found to be particularly easy and yet highly accurate were:

a) direct measurement of PC_N^2 by obtaining pressure vs. volume data for the experimental tube;

b) the use of inexpensive strain gage transducers for accurate measurement of tube diameter changes;

c) the use of a flow source to prescribe boundary conditions that are independent of the tube properties and the pumping system;

d) excitation of the tube in its natural modes to easily visualize non-linear effects.

2. New Theoretical Work

The theoretical contribution involving the most work was of course the series expansion solution. However, several of the more basic ideas used in formulating the physical model are perhaps more important. These are:

a) For large wavelength and laminar fully developed flow the shear stress at the wall may be approximated by the shear stress at the wall of a rigid tube having the same flow and flow history.

b) The flow may be regarded as one-dimensional if one accepts small errors in the non-linear momentum terms.

c) Any small motion theory must be linearized about the mean pressurized radius of the experimental tube to correctly account for the variation of wave speed with mean pressure.

3. Conclusions

The power series in ε of (26) was shown to properly describe the non-linear behavior of the governing equations (1,10,6) up to the point where ε^2 becomes significant when compared to one. The error resulting from use of a linear theory can be estimated as the error resulting from truncating the series (26) after the first perturbation. Thus, for a value of ε of about .18, as at the inlet to the human arterial tree, one would expect about an 18% error when using a linear theory.

If the neglect of entry length and turbulence in the friction model is, in fact, the reason for the discrepancy between calculated and experimental results at large Reynolds numbers, even larger errors could result when the model is applied to the arterial tree. The experimental tube was purposely made as long as possible to minimize entry length effects. The arterial tree continually forks and branches within distances that are short compared with the entry length and, as in the experimental tube, it is likely that the flow is turbulent in the large Reynolds number regions.

4. Future Work

The goal of this work and many other works has been to increase our understanding of the mechanical behavior of the arterial

tree. This understanding will be complete when we are able to predict forces and motions at all points when given the input flow and the relevant physical properties. Toward this goal, we must form a physical model which includes all the important phenomena of a real arterial tree.

Some useful future work would be to develop an accurate physical model for the flow at tube junctions and branches and a model for describing fluid friction at higher Reynolds numbers. Rubber tube experiments should be partially helpful in such studies because the careful experimenter can isolate the particular phenomena being studied by a proper choice of the experimental parameters. This work is primarily for the fluid dynamicist.

The physiologist can provide information of another type. It must be decided whether the approximation $P = f(A)$ is valid for real arteries. If the relation is not valid, for example because of visco-elastic effects, the proper relation must be found. On the other hand, if the pressure is dependent only on tube area, the functional relation should be determined for the various arteries by performing measurements similar to the ρC_N^2 measurement described in chapter 7. These measurements should be performed through the normal range of blood pressure without disturbing the natural supports and constraints provided by the body.

These suggested investigations are thought by the author to be of immediate interest. Some work has been done in each of the areas, but more work, especially good experimental work, is necessary.

REFERENCES

1. Womersley, J.R., "An Elastic Tube Theory of Pulse Transmission and Oscillatory Flow in Mammalian Arteries", WADC technical report 56-614, (1957).

2. Morgan and Kiely, "Wave Propagation in a Viscous Liquid Contained in a Flexible Tube", JASA 26, 323-328, 1954.

3. Personal observation and discussion with medical research workers.

4. Burton, W.E., "Engineering with Rubber", McGraw-Hill, 1949, esp. p. 20.

5. Schlichting, H., "Boundary Layer Theory", McGraw-Hill, 4th ed., p. 229.

6. Crandall, S.H., "Engineering Analysis", McGraw-Hill, 1956, Ch. 6.

7. Fox, P.A., "On the Use of Coordinate Perturbations in the Solution of Physical Problems", doctoral thesis, M.I.T., November 13, (1953).

APPENDIX I

An Analysis of the Error Resulting from the Momentum Flux Approximation.

In this appendix the exact momentum relation will be derived and the momentum flux will be compared with the approximate result for several values of α. We begin by considering the control volume of fig. 33.

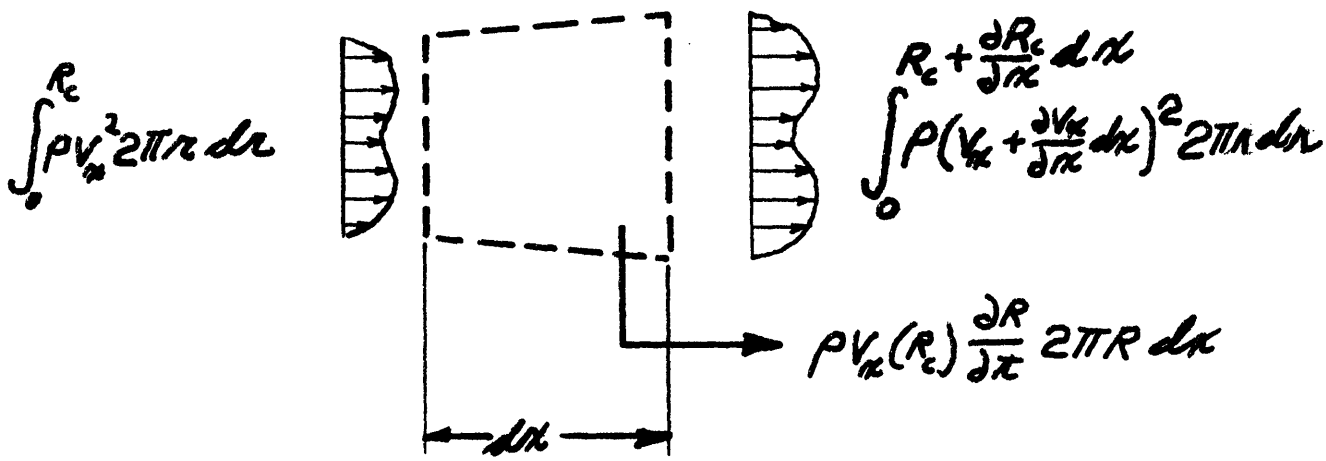

FIGURE 33

The control volume relations for the x direction are

$$\Sigma F_x = \frac{\partial}{\partial t}\int_0^{R_c} \rho V_x 2\pi r\, dr\, dx - \int_0^{R_c} \rho V_x^2 2\pi r\, dr +$$

$$\int_0^{R_c+\frac{\partial R_c}{\partial x}dx} \rho\left(V_x+\frac{\partial V_x}{\partial x}dx\right)^2 2\pi r\, dr + \rho V_x(R)\frac{\partial R}{\partial x} 2\pi R\, dx$$

After neglecting terms of higher order and rearranging the limits on the integrals we obtain

$$\Sigma F_x = \frac{\partial}{\partial t}\left[\int_0^R \rho V_x 2\pi r\, dr\, dx - \int_{R_c}^R \rho V_x 2\pi r\, dr\, dx\right] + \int_{R_c}^{R_c+\frac{\partial R_c}{\partial x}dx} \rho V_x^2 2\pi r\, dr + \int_0^{R_c} \rho \frac{\partial V_x^2}{\partial x} dx\, 2\pi r\, dr + \rho V_x(R)\, 2\pi R \frac{\partial R}{\partial t} dx$$

After applying the rules concerning differentiating integrals with variable limits we obtain

$$\Sigma F_x = \frac{\partial}{\partial t}\int_0^R \rho V_x 2\pi r\, dr\, dx + \frac{\partial}{\partial x}\int_0^R \rho V_x^2 2\pi r\, dr\, dx$$

or by substituting the definitions that

$$\overline{V} \equiv \frac{1}{\pi R^2}\int_0^R V_x 2\pi r\, dr$$

$$\overline{V^2} \equiv \frac{1}{A}\int_0^R V_x^2 2\pi r\, dr$$

we obtain

$$\Sigma F_x = \frac{\partial}{\partial t}(A\overline{V}) + \frac{\partial}{\partial x}(A\overline{V^2})$$

By comparing this result with the approximation that the velocity profile is flat, we see that error is that $\overline{V^2}$ is not equal to $\bar{V}^2$. Figure 34 shows the true momentum flux and the approximate value based on $\bar{V}^2$, as a function of phase angle for various values of α. The curves have been normalized by dividing through by the maximum value for the approximate result.

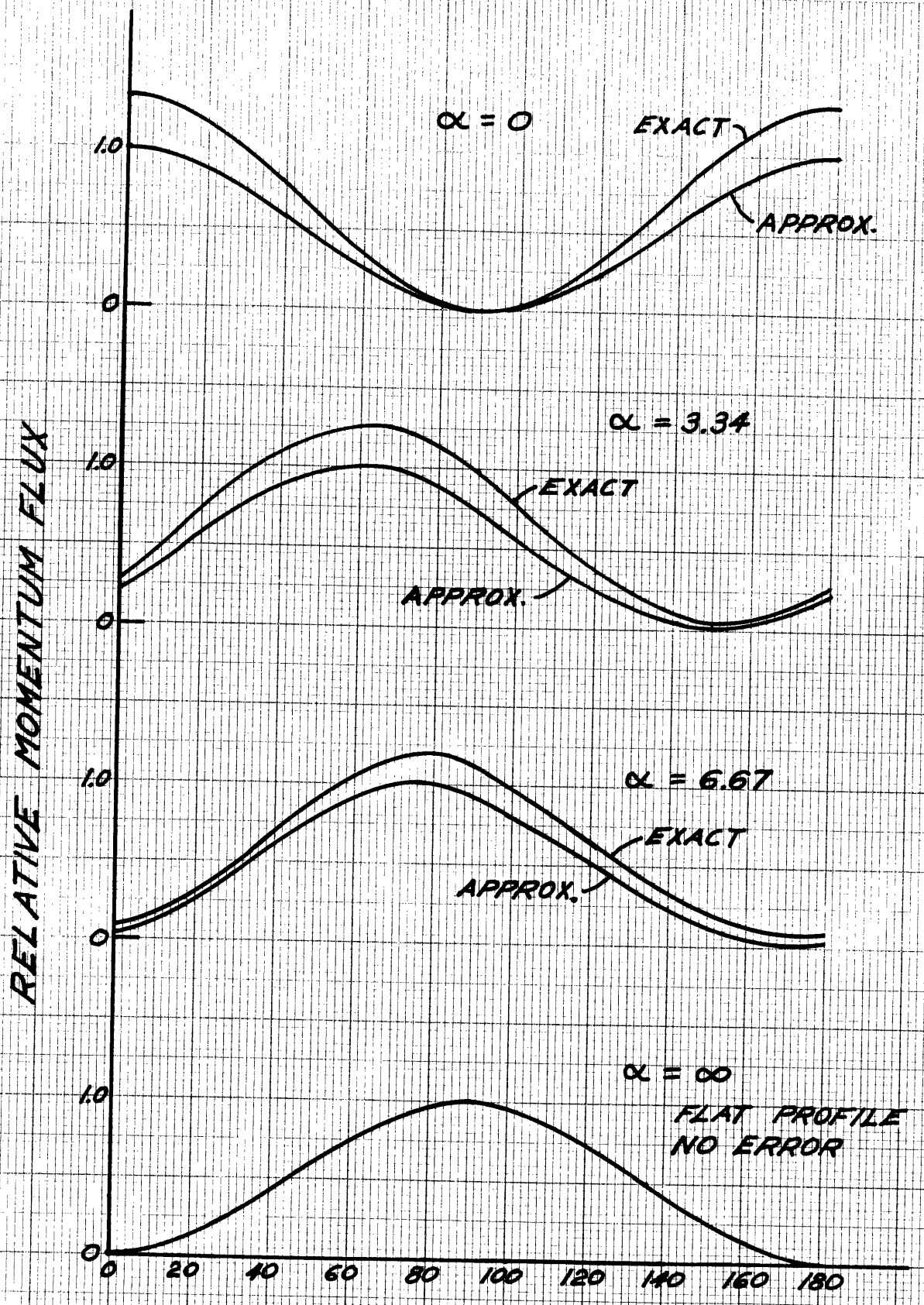
α = 0
EXACT
APPROX.
1.0
0
α = 3.34
EXACT
APPROX.
1.0
0
α = 6.67
EXACT
APPROX.
1.0
0
α = ∞
FLAT PROFILE
NO ERROR
1.0
0
RELATIVE MOMENTUM FLUX
0 20 40 60 80 100 120 140 160 180
PHASE OF FLOW RELATIVE
TO PRESSURE GRADIENT

FIGURE 34

APPENDIX II

DERIVATION OF THE CHARACTERISTIC EQUATIONS

This derivation follows the method given by Crandall,[6] but is applied to the particular case given by eqs. (1) and (2) below.

$$(1) \qquad \frac{\partial(vA)}{\partial x} + \frac{\partial A}{\partial t} = 0$$

$$(2) \qquad c^2 \frac{\partial A}{\partial x} + A\frac{\partial v}{\partial t} + Av\frac{\partial v}{\partial x} = -\frac{\gamma}{\rho}$$

The directional derivatives of v and A along an arbitrary direction s in the x-t plane are

$$(3) \qquad \frac{\partial v}{\partial s} = \frac{\partial v}{\partial x}\frac{\partial x}{\partial s} + \frac{\partial v}{\partial t}\frac{\partial t}{\partial s}$$

$$(4) \qquad \frac{\partial A}{\partial s} = \frac{\partial A}{\partial x}\frac{\partial x}{\partial s} + \frac{\partial A}{\partial t}\frac{\partial t}{\partial s}$$

These four equations can be assembled into the matrix equation below.

$$(5) \qquad \begin{bmatrix} A & 0 & v & 1 \\ Av & A & c^2 & 0 \\ \frac{\partial x}{\partial s} & \frac{\partial t}{\partial s} & 0 & 0 \\ 0 & 0 & \frac{\partial x}{\partial s} & \frac{\partial t}{\partial s} \end{bmatrix} \begin{bmatrix} \frac{\partial v}{\partial x} \\ \frac{\partial v}{\partial t} \\ \frac{\partial A}{\partial x} \\ \frac{\partial A}{\partial t} \end{bmatrix} = \begin{bmatrix} 0 \\ -\frac{\gamma}{\rho} \\ \frac{\partial v}{\partial s} \\ \frac{\partial A}{\partial s} \end{bmatrix}$$

Equation (5) may be regarded as a set of four simultaneous linear algebraic equations for the derivatives $\partial v/\partial x$, $\partial v/\partial t$, $\partial A/\partial x$ and $\partial A/\partial t$. We seek the characteristic lines for which these derivatives are not uniquely determined by eq. (5). That is, we set the determinate of the coefficients of (5) equal to zero and arrive at the following result.

$$(6) \qquad \frac{\partial x}{\partial s} = (v \pm c)\frac{\partial t}{\partial s}$$

If we call the direction s corresponding to the positive sign α and the other direction β, we can write

$$(7) \qquad x_\alpha = (v+c)t_\alpha$$

$$(8) \qquad x_\beta = (v-c)t_\beta$$

where the subscipts denote differentiation.

If we are considering a characteristic direction where the determinate in (5) vanishes, the right hand column of (5) must be compatible with this to have any solutions at all. By substituting the right hand column for any one of the four columns in the 4 x 4 matrix and setting the resulting determinate equal to zero, we obtain

$$(9) \qquad \frac{\partial v}{\partial s}\left[\frac{\frac{\partial x}{\partial s}}{\frac{\partial t}{\partial s}} - v\right] = -\frac{c^2}{A}\frac{\partial A}{\partial s} - \frac{\gamma}{\rho A}\left(\frac{\partial x}{\partial s} - v\frac{\partial t}{\partial s}\right)$$

Since we are considering the characteristic directions during this calculation, the s derivatives are actually taken in the α and β directions and values for x_α and x_β can be substituted in from eqs. (7) and (8) with the result below

$$(10) \qquad \nu_\alpha = -\frac{c}{A} A_\alpha - \frac{\gamma}{\rho A} \tau_\alpha$$

$$(11) \qquad \nu_\beta = +\frac{c}{A} A_\beta - \frac{\gamma}{\rho A} \tau_\beta$$

These results can be put into a more familiar form by multiplying the α and β equations by $d\alpha$ and $d\beta$ respectively and combining into the form

$$(12) \qquad \frac{dx}{dt} = \nu \pm c$$

$$(13) \qquad d\nu = \mp c \frac{dA}{A} - \frac{\gamma}{\rho A} dt$$

where the α,β notation has been dropped and it must be remebered that the increments in the variable are taken along the characteristic curves.